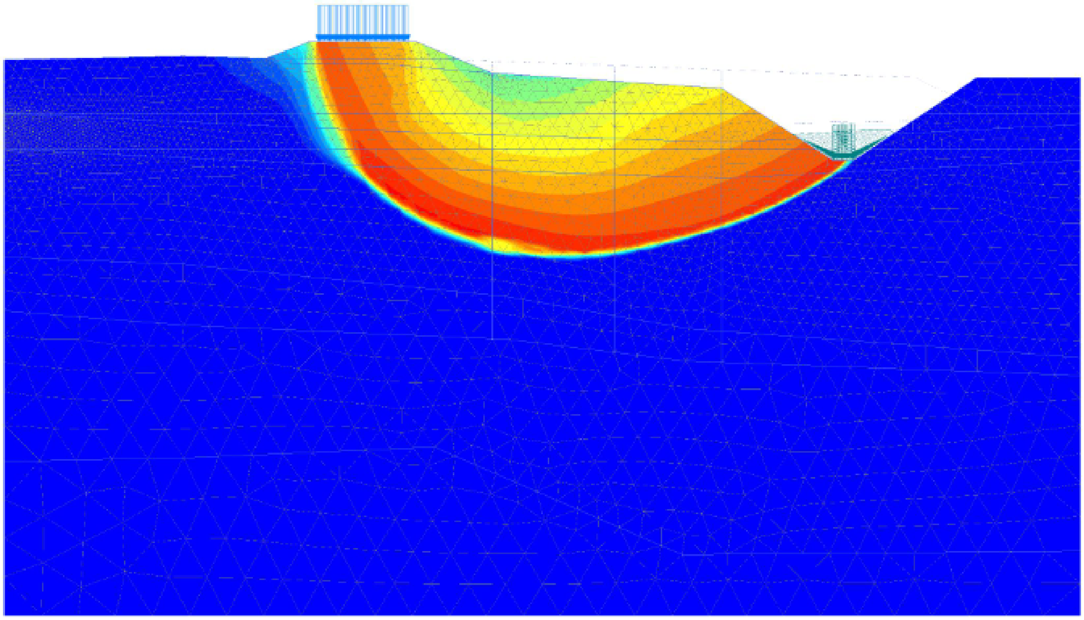

Numerical analyses of the failure of Perniö embankment

Numerical modelling using Creep-SCLAY1S in Plaxis

Master's Thesis in Master Programme Infrastructure and Environmental Engineering

FANNY MOLANDER
CHRISTOFFER ROOS

Department of Architecture and Civil Engineering
CHALMERS UNIVERSITY OF TECHNOLOGY
Master Thesis ACEX30-20
Gothenburg, Sweden 2020

Master's thesis ACEX30-20

Numerical analyses of the failure of Perniö embankment

Numerical modelling using Creep-SCLAY1S in Plaxis

FANNY MOLANDER
CHRISTOFFER ROOS

Department of Architechture and Civil Engineering
Division of Geology and Geotechnics
Chalmers University of Technology
Gothenburg, Sweden 2020

Numerical analyses of the failure of Perniö embankment
Numerical modelling using Creep-SCLAY1S model in Plaxis
FANNY MOLANDER
CHRISTOFFER ROOS

Supervisor: Hannes Hernvall Minna Karstunen, Department of Architecture and Civil Engineering
Examiner: Minna Karstunen, Department of Architecture and Civil Engineering

Master's Thesis ACEX30-20
Department of Architecture and civil Engineering
Geotechnics research group
Chalmers University of Technology
SE-412 96 Gothenburg
Telephone +46 31 772 1000

Cover:

Typeset in LaTeX
Printed by Chalmers Reproservice
Gothenburg, Sweden 2020

Numerical analyses of the failure of Perniö embankment
Numerical modelling using Creep-SCLAY1S model in Plaxis
FANNY MOLANDER
CHRISTOFFER ROOS
Department of Architecture and Civil Engineering
Division of Geology and Geotechnics
Chalmers University of Technology

Abstract

With the increasing population and people travelling with a higher demand for sustainable travelling transport alternatives, the railway network is needed to be developed. In this thesis an earlier performed failure test embankment in Perniö, Finland is analysed and simulated numerically in Plaxis, using the creep-SCLAY1S model. It is discussed however the old railway embankments can handle higher axial load than they were initially buildt for or if reinforcements are needed. The result and discussion in this thesis compare the measured results from the performed failure test with the modelled results performed in this thesis. The compared results were similar except from the displacements and the results show that the old railway has the capacity to carry higher loads than initially predicted.In conclusion, it is discussed however numerical methods are suitable for analysing failure or not. Thus Numerical models are precise and take many parameters and aspects into account when calculating failure the Plaxis tool are calculating until the soil fails and are not able to simulate a load coming from a train.

Keywords: Creep-SCLAY1S, Embankment, Failure test, Numerical model, Soft soil, Perniö, Plaxis

Acknowledgements

We would like to thank our examiner Minna Karstunen for introducing us to the subject and our supervisor Hannes Hernvall for quick response and guidance through the process. We also would like to thank Anders Tegnell and Chalmers University of Technology for have taken responsibility in the though covid-19 situation and for making it possible for us to finish our studies on distance.

Fanny Molander & Christoffer Roos
Gothenburg, June 2020

Contents

Roman letters

c	Cohesion
E	Yong's modulus
E_{50}^{ref}	Secant stiffness in standard drained triaxial test
E_{oed}^{ref}	Tangent stiffness for primary oedometer loading
E_{ur}^{ref}	Unloading/reloading stiffness from drained triaxial test
E_{ur}	Current stress-dependent elastic Yong's modulus
G_0^{ref}	Reference shear modulus at very small strains
K_0	Latheral earth pressure coefficient for over consolidation
K_0^{nc}	K_0-value for normal consolidation
m	Power of stress-level decency of stiffness
M_c	Stress ratio at critical state in triaxial compression
M_e	Stress ratio at critical state in triaxial extension

Greek letters

α_0	Initial anisotropy
χ_0	Initial bonding
$\Delta\varepsilon$	Relative strain
$\dot{\varepsilon}$	Total strain rate
$\dot{\varepsilon}_p^c$	Volumetric creep strain rate
$\dot{\varepsilon}_p^e$	Volumetric elastic strain rate
$\dot{\varepsilon}_q^c$	Deviatoric creep strain rate
$\dot{\varepsilon}_q^e$	Deviatoric elastic strain rate
$\dot{\varepsilon}^c$	Creep strain rate
$\dot{\varepsilon}^e$	Elastic strain rate
ε_{cr}	Creep strain
ε_p	Volumetric strain
ε_q	Deviatoric strain
η	Stress ratio
η_{K0}	Initial stress ratio
γ	Unit weight
γ_{sat}	Saturated unit weight
γ_{unsat}	Unsaturated unit weight
κ^*	Modified swelling index
λ^*	Modified compression index
λ_i^*	Modified intrinsic compression index
μ^*	Modified creep index
μ_i^*	Modified intrinsic creep index
ν'	Poisson's ratio
ν_u	Undrained Poisson's ratio
ω	Absolute effectiveness of rotational hardening
ω_d	Relative effectiveness of rotational hardening
ϕ'	Friction angle
ψ'	Dilatancy angle
ρ	Density
σ_c'	Apparent preconsolidation pressure

σ'_h	Effective horisontal stress
σ_t	Tension cut-off and tensile strength
σ'_v	Effective vertical stress
σ'_{v0}	Effective vertical in-situ stress
τ	Reference time
θ	Lode angle
$\dot{\Lambda}$	Visco-plastic multiplier
ξ	Absolute rate of destructuration
ξ_d	Relative rate of destructuration

Abbreviations

CSS	Current State Surface
FEM	Finite Element Method
FTA	Finnish Transport Agency
ICS	Intrinsic compression surface
MC	Mohr Coulomb
NC	Normally Consolidated
NCS	Normal Compression Surface
OC	Over Consolidated
OCR	Over Consolidation Ratio
POP	Pre-Overburden Pressure
YS	Yield Surface

List of Figures

List of Tables

1

Introduction

Over time the need for more effective transport systems has been an important factor in the infrastructure system of most parts of the world. This is no exception for the Scandinavian countries (Eckhardt and Rantala, 2012). With an increasing population, the transport systems need to be up to date and be able to handle higher loads and more dense traffic (Eckhardt and Rantala, 2012). The first railway in Finland was built in 1869 and many of the railways in Finland are built before the 19th century (Vozniak et al., 2018). With an increasing demand in freight transport with higher axle loads than intended when the railway was built, the capacity of old embankments needs to be investigated. If an old railway is to be rebuilt, would the embankment be able to handle higher axial loads than it was built for or is there a need of reinforcement?

To investigate the stability of an old railway embankment, a failure test of a railway embankment was performed in Perniö, Finland in 2009. The test was set up by the Finnish transport administration to investigate the stability of an embankment on a relatively sensitive clay in situ, to assess the stability of embankments with similar conditions. The test location was in an area with an old railway embankment outside Perniö in South-Western Finland. The test was executed by digging out parts of the old fill from the existing railway and excavating a ditch about 14 meters south of the embankment to direct the failure in the direction of the planned instrumentation. Two weeks after building the ditch, a 0.6-meter high embankment was built on the same location as the old embankment. On top of the embankment, a railway track was built, with a stack of containers placed on beams over the track to simulate four train wagons. These containers were loaded with sand in steps until the embankment reached failure. The embankment was monitored with instruments placed in the test area.

Test data was gathered from the instruments, however, as yet no proper numerical analysis has been made to understand the response. The simulations in Plaxis previously performed by D'Ignazio et al. (2017) have been using the basic hardening model, and the most advanced analyses by Lethonen (2011) with an advanced creep model (Yin et al., 2010), did not rigorously account for the effects of anisotropy and the anthropogenic history on the initial state. Furthermore, a limited amount of soil testing was available. Thus, the starting point for the analyses was not ideal.

By starting from the additional soil tests done on samples nearby, taken after the failure test, in this thesis representative set of model parameters have been derived.

Consequently, all the stages of geological and anthropogenic processes that resulted in the initial state of the soil before loading the embankment to failure have been done step by step. Thus, new insight into to problem has been made by doing a numerical analysis in Plaxis using the Creep S-CLAY1S model (Sivasithamparam et al., 2015), resulting in a more representative simulation of the failure of the test embankment.

1.1 Aim and Objectives

The aim of this thesis is to do a quantitative numerical analysis of the Perniö failure test embankment with an advanced rate-depended model. The analyses aim to complement and improve the previous studies, utilising the unique field data from the failure test of the embankment in Perinö, using the Finite Element Method (FEM) and make reflections of the actual outcome of the failure, to generalise the results.
The following Objectives are set:

- Create a Creep-SCLAY1S model for the Perniö failure test embankment.
- Estimate representative model parameters for the soil profile for the numerical analyses using the available experimental and field data.
- Analyse what model parameters are most relevant or sensitive for the case of the embankment in Finland.
- Analyse the problem with Plaxis and thus assess how analyses with an advanced model can be used as a tool for further analyses of the safety of railway embankments.
- Assess what discrepancies are still remaining when modelling embankment failure on sensitive clays.

1.2 Limitations

The performance of the analysis of the Perniö embankment failure test has some limitations in this report as stated below:

- The simulation will be performed with a 2D model, even though the problem is three-dimensional.
- No additional site investigation will be made, thus only a literature study and analyses of gathered data will be used to create the simulation.
- Results may differ between the simulation and the actual failure test since there are always some uncertainties when modelling materials of a geological origin.

1.3 Methodology

A literature study was performed to get a better understanding of the subject and the case. The literature study mainly consisted of online scientific databases but also printed books and material from previous course ACE150, "Soil modelling and numerical analyses" at Chalmers University of Technology. Due to many recent studies performed in the study area, some earlier performed theses were also reviewed to get a better picture and understanding of the case study and the performed failure test. A more detailed description of the failure test can be found in Chapter 2.

From earlier studies performed at the site, laboratory test, and measurement data was retrieved. This data was analysed, and some parameters were recalculated and back- analysed by simulating the experimental response with the Soil Test Tool in Plaxis. The calculation process and the simulated soil tests are described in detail in Sections 4.1 and 4.2, respectively.

After a satisfactory set of model parameters, a Plaxis model for the Perniö embankment failure test was set up, assuming 2D plane strain conditions. The main soil model used was in modelling the layers where the failure occurs is Creep-SCLAY1S, which is an advanced rate-dependent model, described in Section 3.2.4.

The results from the Plaxis simulations were analysed and the important results based on the set aims and objectives were retrieved, these are described in section 5. The results were mainly graphical with meshes showing displacements, pore pressures, and the mechanics of the soil movements. All of the results were based on the Plaxis calculations. After analysing the results a discussion was made based on the results and from these conclusions could be made answering the questions set in the aims and objectives.

2
Site description

This Chapter aims to give a description the loading history and performed failure test of the study area, including the numerical models used for modelling the failure test of Perniö embankment by other authors.

2.1 Perniö embankment

The study area are located in Perniö, in the municipality of Salo, in South-Western Finland. The site is a part of the old railway connecting Helsinki and Turku. In this thesis, the study area, with cross section seen in Figure 2.1 will be referred to as Perniö embankment failure test site.

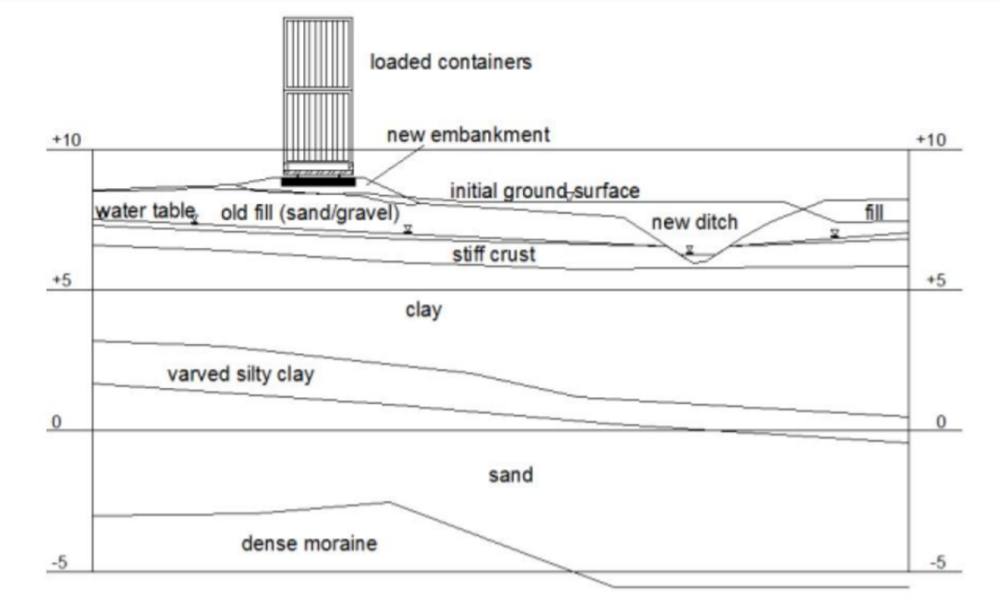

Figure 2.1: Cross section of the test site (Mansikkamäki, 2015)

In this thesis the soil layers, presented in Figure 2.1 will be named as follow:

- New embankment = New fill
- Old fill = Old fill
- Dry crust = Dry crust
- Soft clay = Clay layer 1
- silty clay = Clay layer 2
- sand and dense moraine = moraine

2.1.1 History and geology of the study area

The soil conditions on the test site are mainly consisting of highly sensitive and lightly overconsolidated clay due to ageing effects. The studied embankment that was driven to failure was buildt on top of an old railway build from the 1960s (Lehtonen et al., 2015). Figure 2.1 shows a cross-section of the studied embankment where the old railway rested on soil consisting of old fill, dry crust, soft clay, varved clay, and a layer of sand/moraine, respectively. To perform the failure load test on the embankment a new railway embankment was built on top of the old railway and then brought to failure using sand-filled containers.

2.1.2 Full scale failure test

In Perniö, a full-scale railway failure embankment test was performed in 2009, to collect full-scale monitoring data and assess the reliability of calculation methods for the stability of old railways embankments. The test was performed by Tampere university together with the Finish Transport Agency (FTA). Before the loading of the embankment to failure, a site investigation program was performed in the study area. Figure 2.2 shows the investigation program, which consisted of 24 weight soundings, 13 vane shear tests, and 19 CPTU tests to characterise the soil underneath the test embankment. Also conventional laboratory triaxial and oedometer tests were performed.

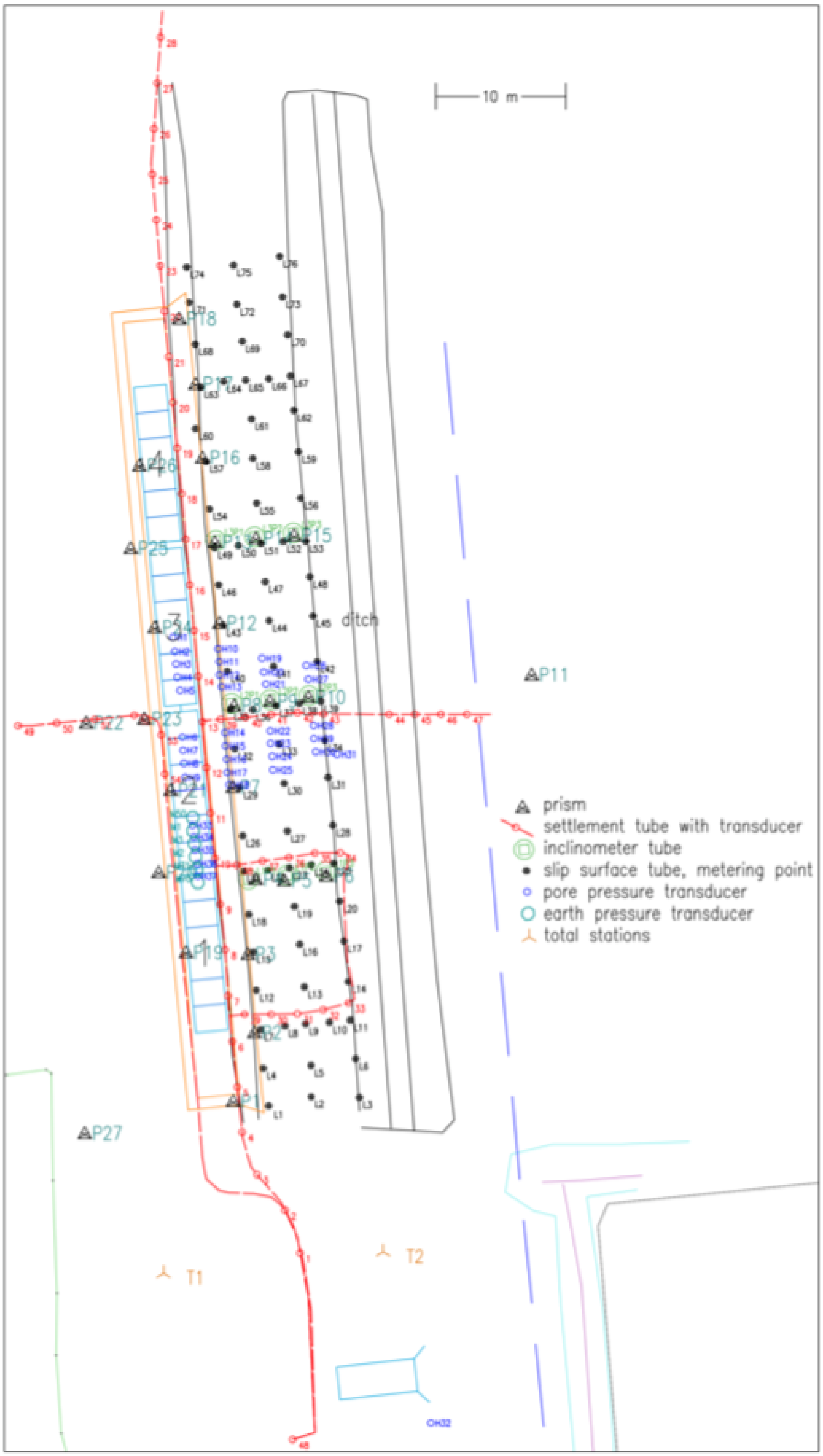

Figure 2.2: *Measurement instrumentation location. (Lethonen, 2011)*

2.1.3 Loading of the failure embankment

To perform the failure test, a new 0.6 m high and 60m long embankment was buildt on top of the old embankment. The old embankment was considered to be too weak to be representing an operational railway embankment. Additionally, a ditch was excavated on the side of the embankment to control the collapse. The side slope of the embankment was around 1:2 and the ditch had a slope of 1:15.

.

Figure 2.3: *Perniö failure embankment (Lethonen, 2011)*

On top of the new embankment four containers were placed, as illustrated in Figure 2.3, and thereafter loaded stepwise by filling the containers with sand. The loading began on 20 October 2009 at 15:30, defined as t=0(hours):00(min). Each loading step was an incremental loading of 15t to each container, corresponding to an incremental trainload of 4.7kPa.
To ensure that the failure would occur at the centre of the embankment, the two middle containers in Figure 2.3 was loaded with 24kPa and the outer containers with 21kPa during the first time step. Thereafter, a load of approximately 5.5kPa/h was added to each container until the middle containers were loaded with 87 kPa, and the outer with 85 kPa. This load was higher than expected based on initial analyses and was the maximum load that could be applied. Loading was halted at t=28:04 and failure occurred at t=29:57.

2.1.4 In situ measurements

When the failure test took place in 2009, there were nearly 300 measurement targets installed on and around the embankment. These points were chosen to get an accurate idea of the ground movements at surface on the soils during the test from the start of loading to the failure. Figure 2.2 shows a top view of the site with all the measurement instruments included.

The instrumentation installed on site consisted of:

- 37 Pore pressure transducers installed to measure excess pore pressure in the expected failure zone. Each transducer was placed in clay layer 2 with a 0.25 meter vertical space to minimise the soil disturbance.
- 3 horizontal fluid-filled flexible plastic settlement tubes containing pressure transducers. The tubes were placed in the failure zone to calculate the settlement in given points. The longest tube was 110 meters long with 28 transducers placed under the embankment at the failure side. The second-longest tube was 70 meters long and included 6 transducers. The third tube was 65 meters long with 19 transducers.
- Two total stations for monitoring surface displacements automatically during the experiment.
- 9 inclinometers were installed in three transverse lines between the ditch and the embankment to measure the horizontal displacements in the soil.
- Earth pressure transducers were installed under the embankment in the fill at a level of +7.5 meter to measure the vertical stress under the embankment.
- 76 slip indicators, installed between the embankment and the ditch to estimate the slip surface depth.
- 32 strain gauges for weighting the containers.

3

Background

In this chapter, the theoretical and technical findings from the studied literature will be presented. The chapter starts with explaining the behaviour of soft soils and responses from loading and unloading, focusing on embankments on soft soils. Further, the chapter presents some different numerical models and explain their differences.

3.1 Soft soils

Soft soils are common in many places in Scandinavia. The stress-strain behaviour of soft soils bears some similarities with the stress-strain behaviour of metals but with one important difference, soil is not a continuum but a multi-phase material with solids and voids. The large amount of voids filled up with (usually) water and air which makes the deformations of soils larger than those of metals that must be taken in to account when describing soils (Wood, 1990).

Soil consists of small particles connected by molecular forces which also affects the ratio of deformations and is even higher for soft clay with a high void ratio. The deformations of soil depending on the soil structure and the parameters connected to its composition as density, organic content, water content, grain size, and mineral composition (Larsson, 2008).

Soil deformations consist of both changes in shape (shear strains) and volume (volumetric strains), and the magnitude of the deformations varies. Further, the pore pressure affects the magnitude of the deformations. The pressure affects the relations between the shear stress and normal effective stress, and large excess pore pressure may result in large shear deformations (Larsson, 2008).

The hydraulic conductivity, k, which geotechnical engineers refer to as permeability describes how fast water can flow through the material. For fine-grained soils, such as clays, which consist of very small particles compared to sand, the permeability is slightly low. Sand have a permeability with the magnitude of 10^{-5}m/day while clay have a permeability with the magnitude of 10^{-9} m/day.

Soil deformations can be divided into immediate deformations and time-dependent deformations. Time-dependent deformations consist of consolidation and creep. Consolidation is deformations due to volume reduction caused by the flow of water and is thus associated with a change in effective stress. The classic theory of consolidation was developed by Terzaghi (1923), Figure 3.1 shows the primary and secondary consolidation curve, also called the consolidation curve which will be described in more detail in section 3.1.1. For settlement calculations, it is of importance to take into account the stress history and deformation history in situ of the soil to optimize safety conditions (Meijer and Åberg, 2007). This applies both for consolidation and creep.

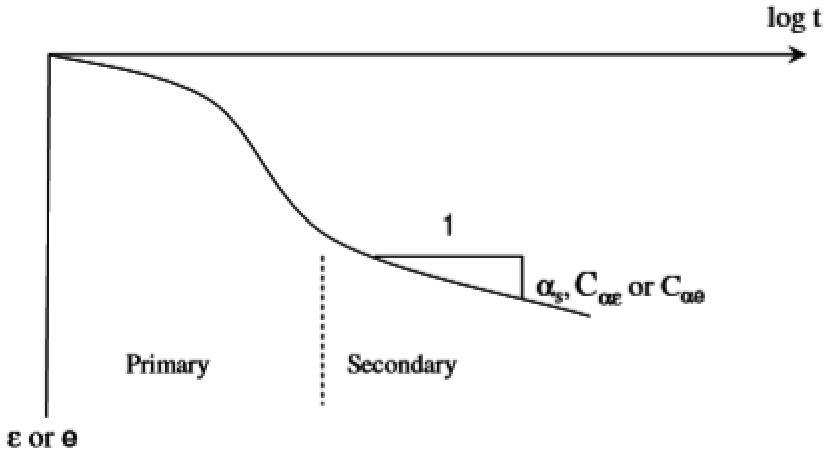

Figure 3.1: *Primary and secondary consolidation curve (Mats Olsson, 2010).*

Immediate deformations for undrained soils consist of shear strain only, and if drainage is enabled, both volume change and shape changes (Larsson, 2008), resulting in both volumetric and shear strains.

3.1.1 Creep

The time-dependent deformations of soils consist of both consolidation and creep. Consolidation is described in the previous section and creep will be described in more detail in this section.

Creep, also called secondary consolidation, can be described as deformations with time, under constant effective stress, and no change in excess pore pressure (Wood, 1990). The deformations from time-dependent creep are controlled by viscosity and is characterized by a coefficient for secondary consolidation C_α. This coefficient describes the linear relation between creep deformations and the logarithm of time and is commonly used in most other countries than Sweden. Hence in Sweden its most common to describe creep with α_s which can be derived as the slope of the consolidation/compression curve defined in equation 3.1 and equation 3.2. Figure 3.1 visualize the consolidation/compression compression curve which is the result from Incremental Oedometer tests.

$$C_\alpha = \frac{\Delta e}{\Delta log(t)} \tag{3.1}$$

$$\alpha_s = \frac{\Delta\varepsilon_{cr}}{\Delta log(t)} \tag{3.2}$$

α_s describes the creep deformation development during time, and the results from oedometer tests in laboratory suggest that creep is strongly dependent on the effective stress. The apparent creep rate increases between $0.8\sigma'_c$ and $1.0\sigma'_c$, thus accelerating as we approach the apparent preconsolidation pressure. Creep can be assumed to be insignificant until a certain deformation of $0.8\epsilon_{cr}$ is reached, and thereafter increases until its maximal deformation, ϵ_{cr} (Meijer and Åberg, 2007).
Janbu, 1969 presented a theory, where the creep deformations were described with a time resistance number r, defined in equation 3.3.

$$r_s = \frac{dR}{dt} \tag{3.3}$$

where R is the time resistance defined as:

$$R = \frac{dt}{d\epsilon} \tag{3.4}$$

Laboratory tests shows a relation with time and that the time resistance R is increasing after a certain reference time t_r, corresponding to the time where the excess pore pressure have equalised and primary consolidation end (Meijer and Åberg, 2007). This is visualised in Figure 3.2.

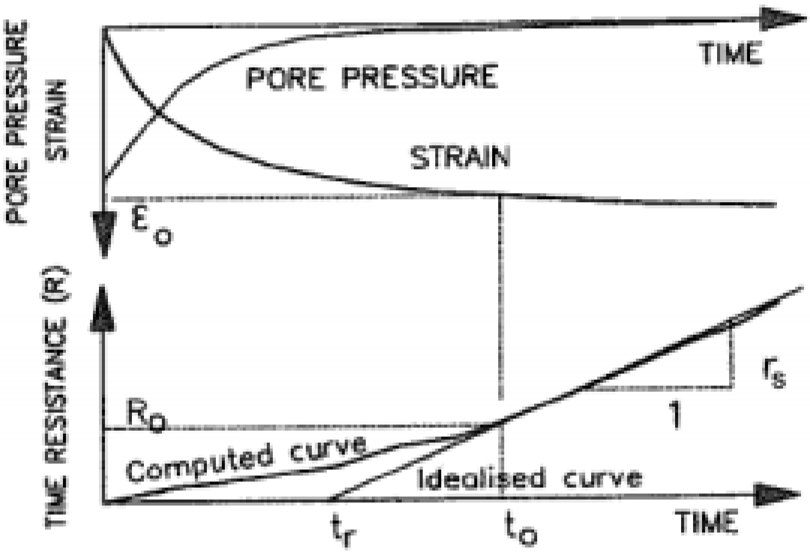

Figure 3.2: *Time resistance R with time svanø, 1991*

Were after the time resistance can be described as:

$$R = r_s \cdot (t - t_r) \tag{3.5}$$

where r_s refer to the time resistance numer and t_r is the reference time.
The creep strain due to time can be expressed as a integration over time from t_0 to, t according to equation 3.6, where t_0 is the time where R is increasing linearly with time (Meijer and Åberg, 2007).

$$\Delta\varepsilon_{cr} = \frac{1}{r_s}\int_{t_0}^{t}\frac{dt}{(t-t_r)} = \frac{1}{r_s}\cdot ln\frac{(t-t_r)}{t_0-t_r} \tag{3.6}$$

3.1.2 Embankments on soft soils

Building embankments on top of soft soil is still a challenge (Karstunen et al., 2006). As cities are growing, there is a need for building in areas that were earlier considered to be unsuitable for construction. For geotechnical engineers, there are challenges such as the stability of the slopes, low bearing capacity, and differential settlements. For constructing embankment on soft soil there are many approaches, summarised in Figure 3.3, where some of the methods improve either settlements or stability, but most of them affecting both settlement and stability (Almeida and Marques, 2013).

Which technique to use in a certain project depends on different factors as, cost, geotechnical deposits, area use and construction timeline. Some of the methods are not suitable for urban areas, such as removal of soft soil, given the lack of disposal areas.

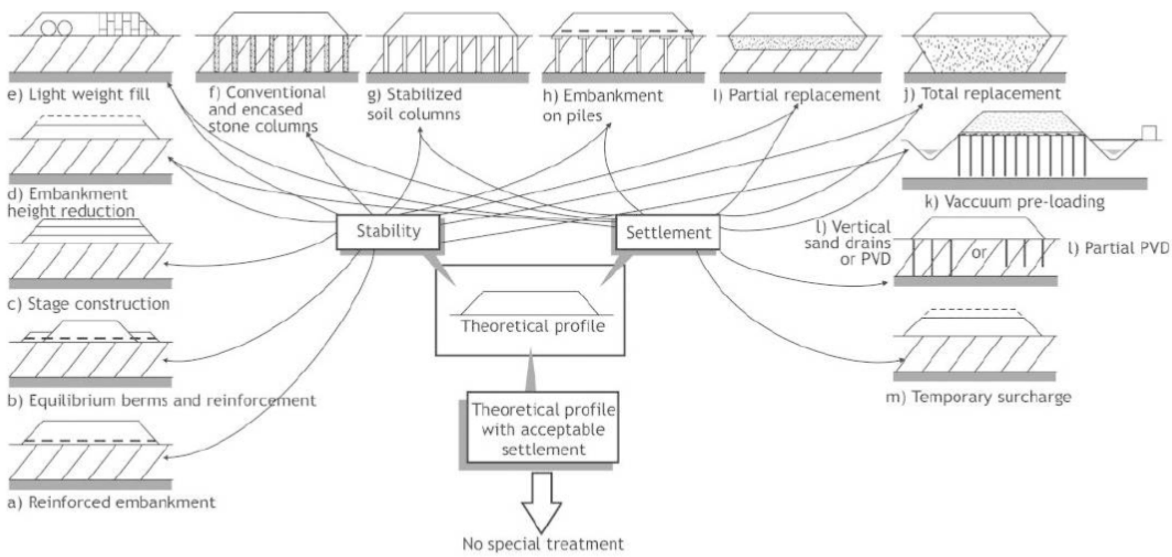

Figure 3.3: *Methods for construct embankments on soft soil (Almeida and Marques, 2013).*

Another challenge when constructing on soft soils is the placement of the equipment. In very soft soils where the support capacity is very low a construction platform needs to be built (Almeida and Marques, 2013). A working platform is a constructed area next to the building area, where to place the heavy equipment. In cases with very soft soils, the working platforms are often built using geotextiles reinforcement.

Regardless of the chosen construction method, there is a need of monitoring the performance of the constructed embankment to avoid failure during and after construction and to ensure the embankment's function. Vertical and horizontal displacements are often monitored to avoid detrimental effects on the surroundings. This can be monitored with inclinometers and settlement plates. Pore pressures are something that also needs to be monitored, this is made easy with piezometers (Almeida and Marques, 2013).

3.2 Numerical models

To numerically simulate the embankment failure test, Plaxis 2D was used. Plaxis is a program, using the Finite element method, to analyse deformations and stability of soils.
There are several ways of expressing the stress-strain relationship for soils. This expression is also called the constitutive model and there are several classes or types of constitutive models (Amavasai and Karstunen, 2017). Four of the most commonly used types of constitutive models, visualized in Figure 3.4 are: the rigid-perfectly plastic, the Elasto-plastic perfectly plastic, the Elasto-plastic hardening and the elastoplastic softening models which can be used for numerical modelling.

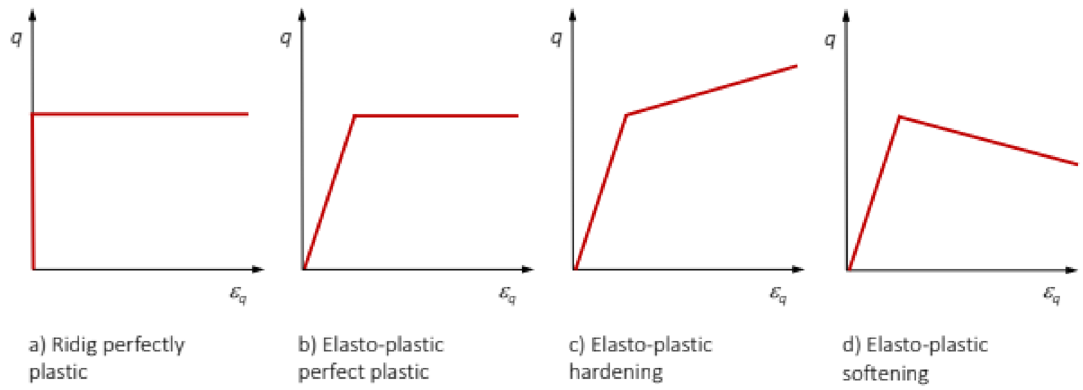

Figure 3.4: *Four constitutive models (Amavasai and Karstunen, 2017).*

Independently, whichever model is used there are four essential components included in elasto-plastic models. These form of components vary between the models, but the concept are the same. The necessary components in all elasto-plastic constitutive models are:
The elastic laws, which is defined in its simplest form from Hooke's Law of Isotropic elasticity as:

$$\varepsilon_x = \frac{1}{E}(\sigma_x - \nu\sigma_y - \nu\sigma_z) \tag{3.7}$$

$$\varepsilon_y = \frac{1}{E}(-\nu\sigma_x + \sigma_y - \nu\sigma_z) \tag{3.8}$$

$$\varepsilon_z = \frac{1}{E}(-\nu\sigma_x - \nu\sigma_y + \sigma_z) \tag{3.9}$$

Equation 3.7-3.9 describes the calculation of the strain where E is Young's modulus and ν is the Poisson's ratio. Shear strains are produced and a shear modulus, G is inserted into the model. The shear modulus, G describes the relation between the shear strain τ and the angle change γ. What parameters to insert depends on the material model and the soil properties, but commonly used elastic parameters are:

- Young's modulus, E
- Shear modulus, G
- Poisson's ratio, ν
- Bulk modulus, K

The yield surface is used to delimit the elastic domain. The elastic domain is inside the yield surface and the plastic is on the surface, if the stress state is outside the yield surface, it is an impossible state.

The yield surface looks different between the models and thus different input parameters are used. In the Perfectly plastic case, the yield surface is fixed. The hardening plasticity has an expanding yield surface and the softening plasticity has a contractive yield surface. This contraction or expansion is controlled by the hardening parameter h_i and the yield surface can be expressed as:

$$f'(\sigma'_{ij}) \tag{3.10}$$

for a fixed Yield surface and

$$f'(\sigma'_{ij}, h_i) \tag{3.11}$$

for a contractive and expanding yield surface. also expressed as:

$$f'(p', q, p'_0) \tag{3.12}$$

where p'_0 is the hardening parameter.

The yield surface is a generalization of the 1D case and is visualized in figure 3.5

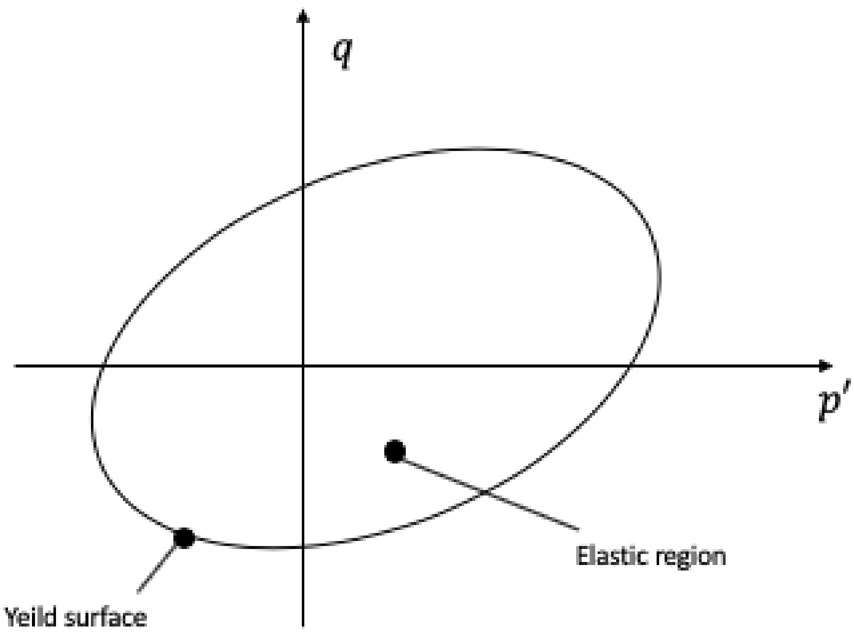

Figure 3.5: *Yield surface description.*

The hardening laws, which are connected to the size and the change in orientation of the yield surface (Amavasai and Karstunen, 2017). In the expression of the yield surface in equation 3.11 and 3.12, the hardening parameter h and p'_0 control the expansion or contraction of the yield surface during plastic deformations.
The hardening rule and the hardening parameter is expressed as:

$$p'_0 = p'_0(\varepsilon^p_p, \varepsilon^p_q) \tag{3.13}$$

Compared to the standard numerical models in Plaxis, the hardening rules of Creep-SCLAY1S also takes into account the rotation of the yield surface which will be described more detailed in section 3.2.4.
The fourth component is **the flow rule**. This is the direction of the plastic flow. The flow rule can be non-associated or associated. In associated flow, the plastic flow is normal to the yield surface. In non-associated flow, a separate plastic potential surface g is introduced.
expressed as:

$$d\varepsilon^p_p = d\lambda \frac{\partial g}{\partial p'} \tag{3.14}$$

$$d\varepsilon^p_q = d\lambda \frac{\partial g}{\partial q'} \tag{3.15}$$

Where g is the plastic potential, and the first term in equation 3.14 and 3.15 describes the magnitude of the plastic deformations while the second term in the equations control the plastic deformation direction.

3.2.1 Mohr-Coulomb model

One commonly used model is the Mohr-Coulomb model which is an elastoplastic-perfectly plastic model. The model behaves purely linearly elastically until failure is reached and after failure deformations behave perfectly plastic. The Mohr-Coulomb model is not suitable for normally consolidated (NC) or overconsolidated (OC) soft clays, which exhibit bi-linear response, therefore it is used for stiff soil layers without significant volume change during shearing (Amavasai and Karstunen, 2017). The parameters of importance for the Mohr Columb model are shown in table 3.1.

Table 3.1: *Input parameters for Mohr Columb model.*

E	kN/m^2	Young's modulus
v	%	Poissons ratio
c	kN/m^2	Cohesion
ϕ	°	Friction angle
ψ	°	Dilatancy angle
σ_t	kN/m^2	Tension cut-off and tensile strength

3.2.2 Hardening soil model

More suitable for normally consolidated and overconsolidated clays are the constitutive models with elasto-plastic hardening. The Hardening Soil Model contains two main types of hardening, both shear hardening, and compression hardening, which are used for model irreversible plastic strains ("PLAXIS Material Models CONNECT Edition V20", 2015).

The Hardening Soil model takes into account for stress dependency of soil stiffness. Compared to an elastic perfectly plastic model as Mohr-Coulomb, the Hardening Soil model has a yield surface which is not fixed but can expand due to plastic straining ("PLAXIS Material Models CONNECT Edition V20", 2015).

The expanding yield surface is divided into three parts which are, the cap yield surface, the shear hardening yield surface and the Mohr Coulomb yield surface, all visualised in Figure 3.6 (Amavasai and Karstunen, 2017).

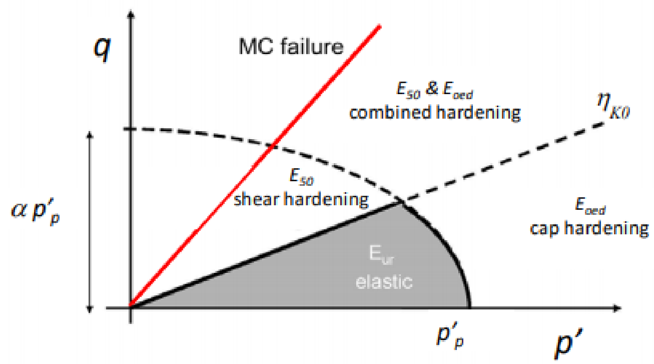

Figure 3.6: *Yield surface of the hardening soil model (Amavasai and Karstunen, 2017).*

The cap surface is assumed to have an associated flow rule and its size is controlled by the over consolidation ratio (OCR), or alternatively the pre overburden pressure (POP). The size of the shear hardening is defined with the coefficient of lateral earth pressure at rest, K_0^{NC} which can be determined with Jaky's formula:

$$K_0^{NC} = 1 - sin(\phi_c') \tag{3.16}$$

The stiffness parameters for the Hardening soil model are determined from laboratory triaxial and oedometer tests, as the secant of the unloading-reloading curves, or the tangent of the loading curve, respectively, as visualised in Figure 3.7. From oedometer tests the drained stress-dependent stiffness parameter can be calculated as:

$$E'_{oed} = E_{oed}^{ref}(\frac{\sigma'_y}{p_{ref}}) \tag{3.17}$$

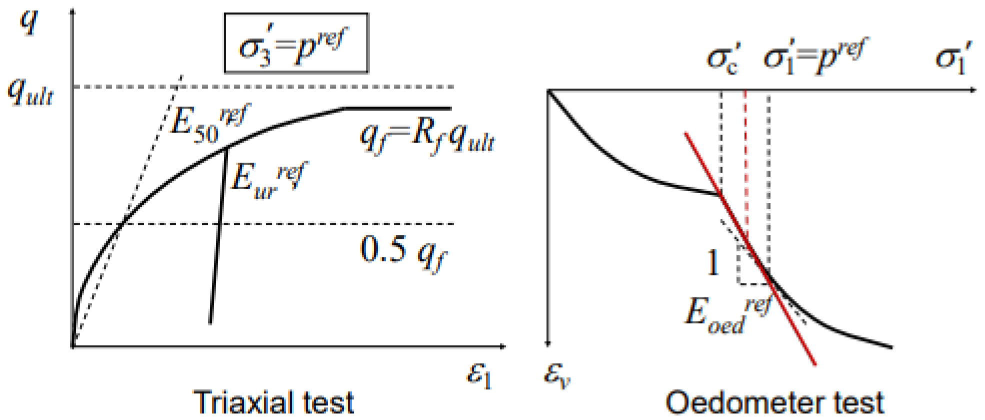

Figure 3.7: *Secant modulus and tangent modulus from triaxial and oedometer loading curves (Amavasai and Karstunen, 2017).*

where p_{ref} is a reference pressure (often assumed to be equal to 100 kPa in Plaxis), assumed to be equal to σ_3' in triaxial test and for oedometer loading the reference pressure are assumed to be equal to σ_1'. Input parameters for Hardening Soil Model are presented in table 3.2

Table 3.2: *Input parameters for Hardening soil model.*

m	-	power for stress-level decency of stiffness
E_{50}^{ref}	kN/m^2	Secant stiffness in standard drained triaxial test
E_{oed}^{ref}	kN/m^2	Tangent stiffness for primary oedometer loading
E_{ur}^{ref}	kN/m^2	Unloading/reloading stiffness from drained triaxial test
υ_{ur}	%	Poissons's ratio for unloading-reloading
POP	kN/m^2	Pre overburden pressure
OCR	kN/m^2	Over consolidation ratio

3.2.3 Soft Soil model

The Soft Soil model is a simple model to use for soft, normally consolidated, or overconsolidated soils, even though it is not suited for modeling clays with high sensitivity. The Soft Soil model is an elastoplastic hardening model. The yield surface is elliptical and the size of the yield surface for the soft soil model is defined by the OCR (or the POP) which are defined based on the relation between the preconsolidation pressure, σ'_c and the in situ vertical effective stress, σ'_v alternative for

$$POP = \sigma'_c - \sigma'_v \tag{3.18}$$

The cap yield surface in the Soft Soil model assumes associated flow, and the modified swelling index, κ^*, and compression index, λ^* are used as the stiffness parameters. These indexes are defined as the slope of the curve representing the relation between the volumetric strains and the natural logarithm of the changes in mean effective stress, visualized in Figure 3.8.

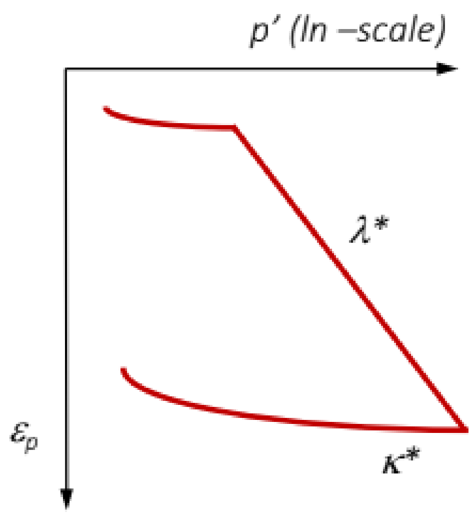

Figure 3.8: *Swelling index and compression index determination (Amavasai and Karstunen, 2017).*

The Soft Soil model also takes the memory of pre-consolidation stress into account. To account for the horizontal effective stresses at yield, the coefficient of lateral earth pressure at rest at normally consolidated conditions is calculated from Jaky's formula, $K_0^{NC} = 1 - sin\phi'_c$ with friction angle at the critical state. Input parameters for the Soft soil model are presented in table 3.3.

Table 3.3: *Input parameters for Soft soil model.*

λ^*	-	Modified compression index
κ^*	-	Modified swelling index
c	kN/m^2	Effective cohesion
ϕ	°	Friction angle
ψ	%	Dilatancy angle
σ_t	kN/m^2	Tensile strength
υ_{ur}	%	Poisson's ratio for unloading / reloading
K_0^{NC}	-	coefficient of lateral stress in normal consolidation
M	-	K_0^{NC}-parameter

3.2.4 Creep-SCLAY1S

Creep-SCLAY1S is a rate-dependent constitutive Plaxis model that can be used in Plaxis for 2D or 3D. The model used in this thesis was developed and implemented at Chalmers in collaboration with NGI (Norwegian Geotechnical Institute) and Plaxis bv. The model is now available as a user-defined model for Plaxis VIP customers. The model accounts for anisotropy via a rotational hardening law and takes both creep and the apparent bonding of sensitive clays into account, which makes it applicable for soft sensitive clays (Amavasai and Karstunen, 2017).

For the flow rules, associated flow is assumed to simplify the elasto-viscoplastic model and this also helps in making it numerically stable. The total strain rate consists of two parts, first an elastic part and then a viscoplastic part. The later is described in eq 3.19. The elastic part are based on Hooke's law and the visco-plastic part represent time-dependent and irreversible strains (Karstunen et al., 2006).

$$\dot{\varepsilon}^c = \dot{\varepsilon}^c_p + \dot{\varepsilon}^c_q = \dot{\Lambda}\frac{\delta p'_{eq}}{\delta p'} + \dot{\Lambda}\frac{\delta p'_{eq}}{\delta q} \tag{3.19}$$

where $\dot{\varepsilon}^c_p$ and $\dot{\varepsilon}^c_q$ is the volumetric and deviatoric creep strain rate, $\dot{\Lambda}$,the visco-plastic multipeler, defined as:

$$\dot{\Lambda} = \frac{\mu_i^*}{\tau}\left(\frac{p'_{eq}}{p'_m}\right)^{\beta}\left(\frac{M_c^2 - \alpha_0^2}{M_c^2 - \eta_{K0}^2}\right) \quad \text{where} \quad \beta = \frac{\lambda_i^* - \kappa^*}{\mu_i^*} \tag{3.20}$$

Where p'_{eq} is the equivalent current stress, μ_i^* is the instrinct creep index and p'_m is the mean effective stress of NCS.

Figure 3.9 visualising the Normal Compression surface of the Creep-SCLAY1S model, which is the boundary between small irrecoverable creep strains and large irrecoverable creep strains. Since the model does not have a purely elastic region. The NCS is assumed to be initially anisotropic, and is simply expressed in triaxial space simply as:

$$f_{NCS} = (q - p')^2 - (M(\theta)^2 - \alpha^2)\,[p'_m - p']\,p' = 0 \tag{3.21}$$

where
p' = mean effective stress
q = deviatoric stress
α = scalar, describing the orientation of the NCS and CSS.
$M(\theta)$ = Stress ratio at critical state as a function of Lode angle

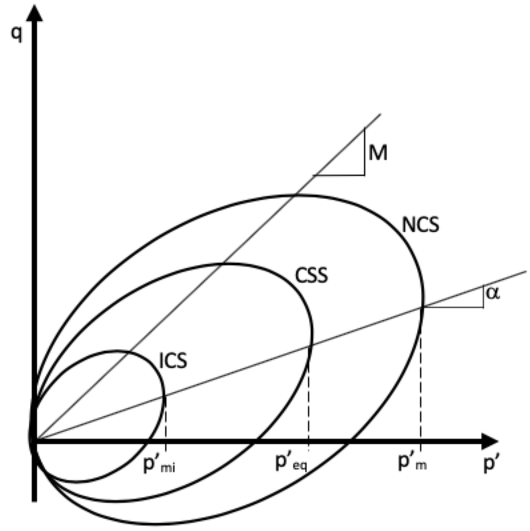

Figure 3.9: *Creep- SCLAY1S model*

Additionally, to the NCS there are two more reference surfaces for the Creep-SCLAY1S model, the current state surface (CSS) and the instinct compression surface (ICS), both illustrated in Figure 3.9. Once the current stress state coincides with NCS, the soil becomes normally consolidated, exhibiting large permanent strains.
Since the Creep-SCLAY1S model is an advanced model and takes many aspects, as creep, bonding, etc into account there are many input parameters which are listed in Table 3.4. A more detailed description of parameter determination can be seen in section 4.2. Input Parameters for Creep-SCLAY1S can be sen in table 3.4.

Table 3.4: *Input parameters for Creep-SCLAY1S model.*

υ'	%	Poisson's ratio
λ_i^*	-	Modified instrinct compression index
κ^*	-	Modified swelling index
M_c	-	Stress ratio at critical state in triaxial compression
M_e	-	Stress ratio at critical state in triaxial extension
α_0	-	Initial anisotropy
ω	-	Absolute effectiveness of rotational hardening
ω_d	-	Relative effectiveness of rotational hardening
χ_0	-	Initial bonding
ξ	-	Absolute rate of destruction
ξ_d	-	Relative rate of destruction
μ_i^*	-	Modified intrinsic creep index
τ	Time	Reference time
POP		Pre overburden pressure
OCR		over consolidation ratio

4
Model setup

In this chapter, the setup of the model that was used for the simulations in Plaxis is presented. This includes the determination of the geometry for the Perniö embankment, the mesh for the calculations, the determination of the soil parameters, how they were calculated, and the calculation steps with measurement placement.

4.1 Geometry

The geometry of the embankment was determined based on reports describing the site (Lehtonen et al., 2015, Lethonen, 2011, Mansikkamäki, 2015). When implementing the geometry in Plaxis, the initial geometry was based on the soil layering before the construction of the embankment failure test. However, for the first step in the calculation, the geometry of the top layer was the dry crust and was horizontal. This to replicate the initial conditions on the site before anything was built and to generate the correct pore pressures for each soil layer. The groundwater level was assumed to be directly above the dry crust (+6,5m). After consolidation in the first calculation step, the actual initial geometry was implemented with the old fill on top of the dry crust. After this, a geometry representing the construction of a ditch east of the embankment was created. This followed by the geometry representing the construction of the embankment. This was the final geometry used for the remaining calculations.

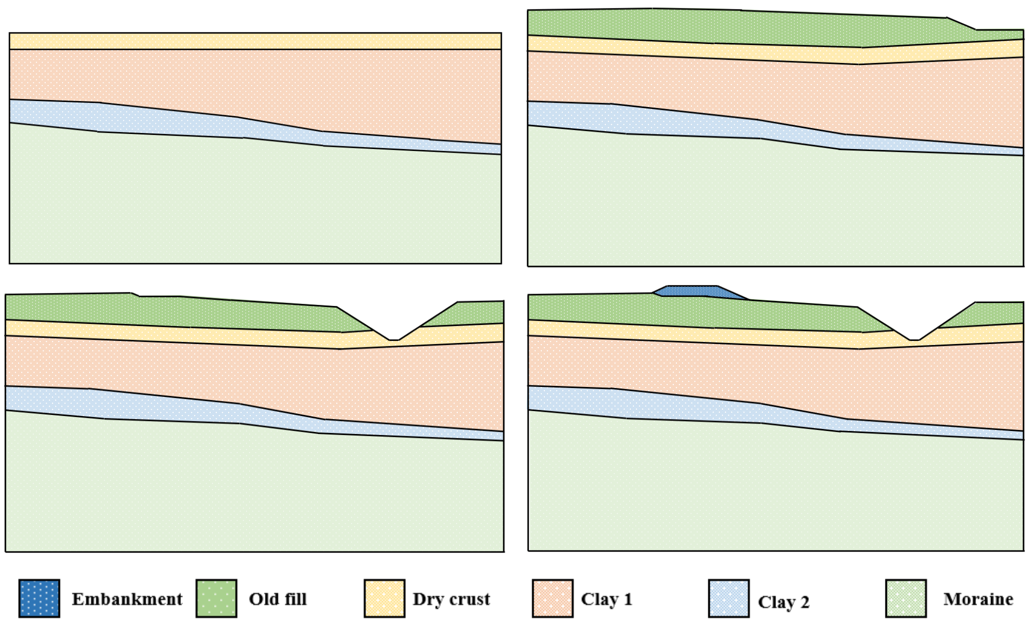

Figure 4.1: *Geometry in Plaxis*

Figure 4.1 shows the geometry built up in Plaxis. The upper left figure shows the initial conditions before construction of the original railway embankment and the upper right figure shows the cross section of the railway embankment with the old fill. The lower figures shows cross sections of the railway embankment after construction of a ditch, and lastly with the new fill on top of the old fill.

4.1.1 Mesh for calculation of Perniö embankment

The mesh used in the Plaxis simulation was set to very fine for the model. For the five top layers: New fill, old fill, dry crust, Clay 1, and Clay 2 the mesh was refined two times. The embankment was also refined two times. This to have more accurate results with smaller elements. In the model, 15 noded elements were used. The mesh set up can be seen in Figure 4.2. The colors in Figure 4.2 represents the size of the elements individually.

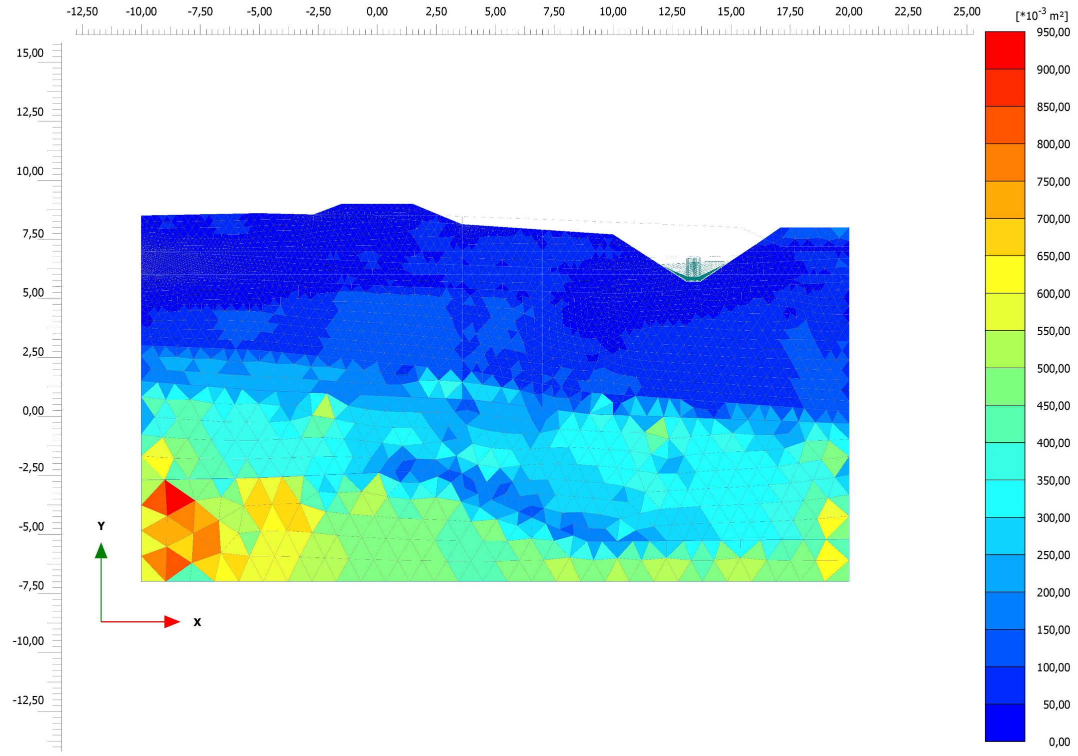

Figure 4.2: *The mesh set up for simulations of the Perniö embankment*

4.2 Parameter determination

When determining the soil parameters, Clay 1 was the layer most focused on. The remaining values for model parameters were retrieved from earlier studies performed by Mataić (2016) and Lehtonen et al. (2015), given these soil layers were not of as big interest for the result as the soft clay layer 1. For Clay 1, the Creep-SCLAY1S model was used and in Section 4.4 the parameter determination for this model is described.

4.2.1 Initial stress parameters

The first parameter taken into consideration was the preconsolidation pressures, σ_c for the dry crust, clay layer 1 and clay layer 2. To evaluate the σ_c is important since it indicates the largest load a soil has been exposed to. σ_c was determined using the Casagrande method. The Casagrande method is explained in Figure 4.3 below.

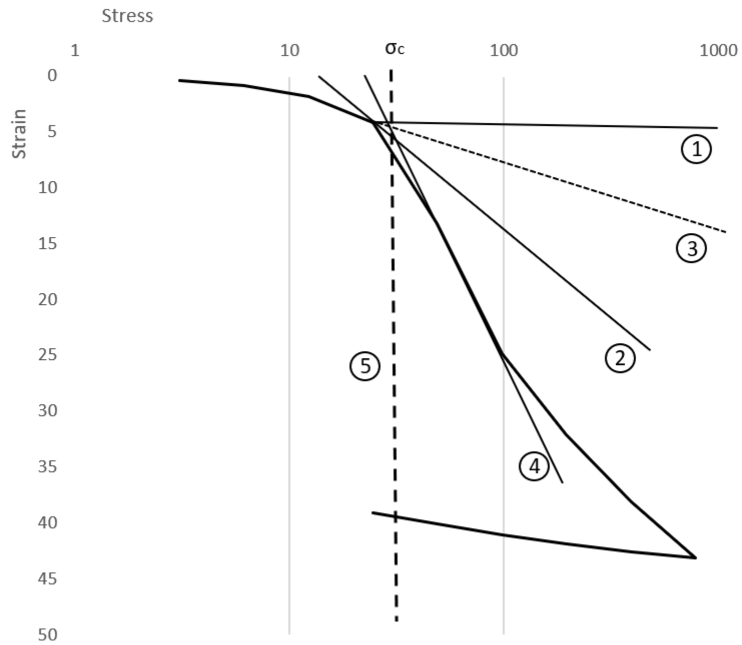

Figure 4.3: *The Casagrande method*

The Casagrande method is based on oedometer tests from soil samples. From the oedometer curve the σ_c can be determined by drawing the following order:

- Line 1: A horizontal line is drawn from the point on the curve with the highest curvature
- Line 2: The tangent line for the point with the highest curvature
- Line 3: The bisector between line 1 and 2
- Line 4: The virgin compression line
- Line 5: The line representing the intersection between line 3 and 4 indicating σ_c

σ_c is crucial to determine the OCR and POP. These are parameters used in the Creep-SCLAY1S model. The effective vertical pressure, $\sigma_v^{'}$ is another crucial parameter. $\sigma_v^{'}$ is determined by multiplying the density of the soil and the depth to get the vertical pressure at a specific depth and then subtracting the water pressure, u at the same depth to get the effective vertical pressure. The POP was determined to be larger directly under the embankment since this part has been subject to larger loads from the old embankment fill and train loads. therefore the POP is decreased in the model for Clay 1 further away from the embankment in the model. The equations for the OCR and the POP can be seen in eq 4.1 and eq 4.2 below respectively.

$$OCR = \frac{\sigma_p}{\sigma_v^{'}} \tag{4.1}$$

$$POP = \sigma_c' - \sigma_v' \tag{4.2}$$

The OCR value was used to determine the lateral earth pressure coefficient at over-consolidated (OC) state, K_0. To calculate K_0 and the lateral earth pressure coefficient at the normally consolidated state, K_0^{nc} the friction angle was determined by field investigation data by Mataić (2016). K_0 and K_0^{nc} indicates the lateral earth pressures (horizontal effective stress) in relation to the vertical earth pressures (vertical effective stress). Eq 4.3 was used to calculate K_0 and eq 4.4 was used to determine K_0^{nc}.

$$K_0 = (1 - \sin\phi') \times \sqrt{OCR} \tag{4.3}$$

$$K_o^{nc} = 1 - sin\phi' \tag{4.4}$$

4.2.2 Conventional parameters

Conventional parameters used in the Creep-SCLAY1S include Poisson's ratio, $\nu^{'}$, the stress ratio at critical state in triaxial compression and extension, M_c and M_e, respectively, the modified intrinsic compression index, λ_i^* and the modified swelling index, κ^*.
$\nu^{'}$ was determined from the field data by Mataić (2016). $\nu^{'}$ is the relation between the vertical and horizontal strain, ε.

Initial values for M_c and M_e were calculated using eq 4.5 and eq 4.6. In the equations the friction angle $\phi^{'}$ was retrieved from the field data by Mataić (2016). M_c and M_e values were later on refined by triaxial simulations performed in Plaxis.

$$M_c = \frac{6sin\phi'}{3 - sin\phi'} \tag{4.5}$$

$$M_e = \frac{6sin\phi'}{3 + sin\phi'} \tag{4.6}$$

The intrinsic slope of the normal compression line, λ_i was calculated by analysing the soil data retrieved from earlier performed soil tests by Mataić (2016) from different depths of the soft clay. The retrieved values of λ_i distributed over the depth were analysed and from this data a mean value of λ_i was determined. After this the initial void ratio e_0 was determined in order to calculate λ_i^* with eq 4.7 below.

$$\lambda_i^* = \frac{\lambda_i}{1+e_0}. \tag{4.7}$$

κ^* was calculated by determining a mean value of of κ similar as for determining λ. After this κ^* was calculated by using the initial void ratio e_0 in eq 4.7. The relation between λ^* and κ^* can be seen in Figure 3.8.

$$\kappa^* = \frac{\kappa}{1+e_0}. \tag{4.8}$$

4.2.3 Anisotropic parameters

Anisotropy is important when modelling soft soils. The anisotropy is results from the shape of the clay particles and their preferred orientation due to the sedimentation and self-weight consolidation (Karstunen and Koskinen, 2008). The initial anisotropy is described with the parameter α_0. α_0 was calculated with eq 4.9 and eq 4.10 (Leoni et al., 2008a).

$$\alpha_0 = \frac{\eta_{k0}^2 + 3\eta_{k0} - M_c^2}{3} \tag{4.9}$$

where

$$\eta_{k0} = 3 \times \frac{1-K_0^{nc}}{1+2K_0^{nc}} \tag{4.10}$$

The initial anisotropy changes when the soil is exposed for plastic straining that is different from the K_0 loading that has been assumed to create the initial anisotropy. The change is represented by the rotation parameters (Leoni et al., 2008b, Amavasai and Karstunen, 2017), ω (rate of rotation) and ω_d (rate of rotation due to deviatoric stress). ω was calculated with eq 4.11 and ω_d was calculated with eq 4.12 below. These parameters were later calibrated with simulated oedometer tests.

$$\omega = \frac{1}{\lambda} \times \ln \frac{10M_c^2 - 2\alpha_0 \times \omega_d}{M_c^2 - 2\alpha_0 \times \omega_d} \tag{4.11}$$

$$\omega_d = \frac{3}{8} \times \frac{4M_c^2 - 4\eta_{k0}^2 - 3\eta_{k0}}{\eta_{k0}^2 - M_c^2 + 2\eta_{k0}} \tag{4.12}$$

4.2.4 Bonding and destruction parameters

Further important effects to consider are the bonding and degradation of bonding between clay particles. The initial bonding, χ_0 depends on the composition of the minerals and the salinity and temperature of the water where the soil was deposited, and subsequent geo-chemical changes (Karstunen et al., 2005). Bonding leads to additional strength in the soil while degradation of bonding leads to less strength. The process of degradation of bonding is that the particles rearrange and slip, the process is called destructuration (Karstunen et al., 2005). Parameters used to calculate degradation of bonding are ξ and ξ_d, where ξ represents the absolute rate of destructuration and ξ_d represents destructuration linked to the deviatoric viscoplastic strain (Sivasithamparam et al., 2015). Eq 4.13 was used to calculate χ_0. ξ and ξ_d were retrieved from soil data by Mataić (2016).

$$\chi_0 = S_t - 1 \tag{4.13}$$

4.2.5 Creep parameters

With the modified intrinsic creep index, μ_i^* and the reference time τ rate-dependency can be modelled in the Creep-SCLAY1S model. μ_i^* is retrieved from an IL oedometer test where the sample is reconstituted or under enough pressure to eliminate all bonding, since μ_i^* is related to pure creep (Amavasai and Karstunen, 2017). τ is the time for each loading step during the IL oedometer test. The determination of μ_i^* can be seen in Figure 4.4.

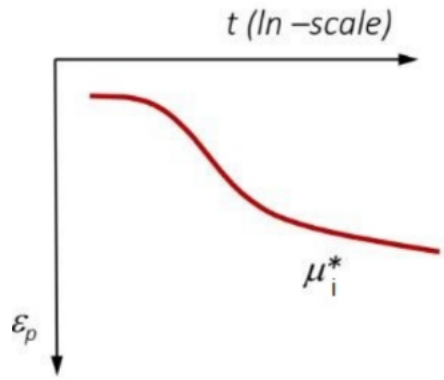

Figure 4.4: *Determination of μ_i^* (Amavasai and Karstunen, 2017).*

4.3 Simulated soil tests

To get a representative model for the clay in Plaxis, the parameters for Clay 1 were analysed by performing simulations of triaxial and oedometer tests in Plaxis. Loading steps and time steps for the simulated tests came from real laboratory tests, performed and analyzed by Mataić (2016).

4.3.1 Oedometer test

From the Perniö embankment failure test site, high-quality undisturbed soil samples were gathered. A series of oedometer tests were performed on these soil samples by Mataić, 2016. In Plaxis a simulation tool was used to recreate these oedometer tests with the earlier calculated parameters for the soft clay, to determine the reliability of the parameters and if necessary, do changes of the parameters. The simulations were performed with four oedometer tests as reference. The graphs used as a reference showed the relation between vertical stress and strain. From the results of the simulations compared to the real-life oedometer tests, parameters were changed to match the real-life tests.

One of the four simulated oedometer tests can be seen in fig 4.5. The dotted line represents the IL oedometer test at 5.47-5.49m depth and the solid line represents the simulated oedometer test at the same depth. To replicate the IL oedometer test results the modified swelling index, κ^* and the modified instrinct compression index, λ_i^* was evaluated to match the inclination of the compression and swelling sections of the curves. The compression sections of the curve are located in the parts with smaller inclination at the beginning of the curve and at the end of the curve and correspond to κ^*. The swelling section of the curve is the section with a larger inclination and corresponds to λ_i^*. By changing κ^* and λ_i^* the inclination of the separate sections could be matched to the IL oedometer test results.

The curvature of the line was determined by evaluating the absolute effectiveness of rotational hardening, ω and the relative effectiveness of rotational hardening, ω_d. ω corresponds to the compression section of the curve and ω corresponds to the swelling section of the curve. The simulated test was fitted as good as possible to the IL oedometer test results and when retrieving a good fit the evaluated parameters were changed in the final input parameters of the Plaxis model.

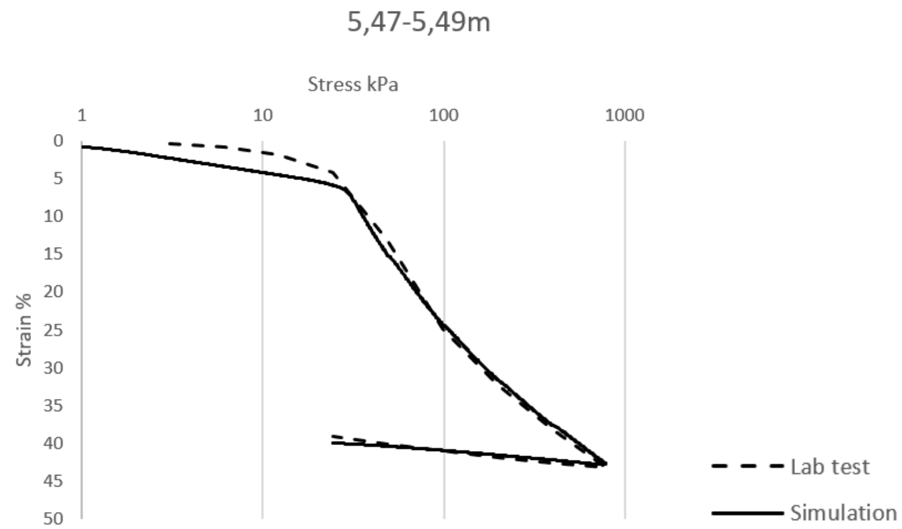

Figure 4.5: Oedometer simulation Plaxis

4.3.2 Triaxial test

The triaxial test simulations were performed similar to the oedometer test simulations. From laboratory data the p'-q curves were analysed and by changing α_0, M_c, ξ_d, the simulated curves corresponded better to the real laboratory test values.

4.4 Input Parameters

The final parameters for each model and soil layer used in the Plaxis model are presented in Table 4.1- 4.4. The Flow parameters for each soil layer are presented in Table 4.5.

Table 4.1: *Final Plaxis input parameters using the Mohr Coulomb model*

	Dry crust	**Moraine**
General		
Type	Drained	Drained
Density unsaturated [kN/m^3]	17	14
Density saturated [kN/m^3]	17	15
Parameters		
E'[kN/m^2]	1*10^4	2*10^4
v'	0.35	0.35
c' [kN/m^2]	3	0.345
ϕ' [°]	34.6	36
ψ [°]		2
Tension cut-off	yes	yes
Initial		
K_0 determination	0.62	Automatic
OCR [kN/m^2]	2.09	

Table 4.2: *Final Plaxis input parameters using the Hardening soil model*

	Embankment	**Old fill**
General		
Type	Drained	Drained
Density unsaturated [kN/m^3]	21	19
Density saturated [kN/m^3]	21	19
Parameters		
v'	0.2	0.2
E_{50}^{ref} [kN/m^2]	1*10^5	2*10^4
E_{oed}^{ref} [kN/m^2]	1*10^5	2*10^4
E_{ur}^{ref} [kN/m^2]	2.5*10^5	6*10^4
m	0.5	0.5
c' [kN/m^2]	1	0.2
ϕ' [°]	38	35
ψ [°]	8	5
p_{ref}	100	100
K_0^{NC}	0.38	0.43
Tension cut-off	yes	yes
Initial		
K0 determination	Automatic	Automatic
OCR [kN/m^2]	1	1
POP [kN/m^2]	20	20

Table 4.3: *Final Plaxis input parameters using the Soft soil model*

	Clay 2
General	
Type	Undrained A
Density unsaturated [kN/m^3]	16
Density saturated [kN/m^3]	16
Parameters	
v'	0.15
c' [kN/m^2]	1
ϕ' [°]	34.6
K_0^{NC}	0.73
M	1.027
Tension cut-off	yes
κ^*	2*10^{-3}
λ_i^*	0.1
Initial	
K0 determination	0.5
OCR [kN/m^2]	1.33

Table 4.4: *Final Plaxis input parameters using the Creep-SCLAY1S model*

	Clay 1
General	
Type	Undrained A
Density unsaturated [kN/m^3]	14
Density saturated [kN/m^3]	15
Parameters	
v'	0.2
ϕ' [°]	34.6
κ^*	1.65*10^{-3}
λ_i^*	6.375*10^{-3}
M_c	1.4
M_e	0.95
ω	52
ω_d	0.95
ξ	14.5
ξ_d	0.3
τ[hours]	24
μ_i^*	2.6*10^{-3}
Initial	
K0 determination	0.52
OCR [kN/m^2]	1.43
POP [kN/m^2]	9-14
α_0	0.4
χ_0	38

Table 4.5: *Final Flow parameters for each soil layer*

	Embankment	**Old fill**	**Dry crust**	**Clay 1**	**Clay 2**	**Moraine**
Flow parameters						
Use defaults	None	None	From data set	From data set	From data set	None
e int	0.5	0.5	2.8	2.35	0.5	3
$k_x [m/h]$	4.16	0.83	$7.2*10^{-6}$	$1.8*10^{-5}$	$1.08*10^{-5}$	0.042
$k_y [m/h]$	4.16	0.83	$7.2*10^{-6}$	$1.8*10^{-5}$	$1.08*10^{-5}$	0.042
c_k	0.25	0.25	1.4	1.175	0.25	1.5

4.5 Phases and loading steps

The embankment failure simulation was calculated in 48 steps. The steps are described in table 4.6 below. The first four steps are representing the construction of the test. Steps 5-48 are the loading and resting phases. The loading and resting steps were determined by reviewing the execution of the failure test from the report by Lehtonen et al., 2015. In Figure 4.6 the loading and resting steps are presented. After three hours of loading the test was paused as shown in Figure 4.6. This since it was dark during these hours and difficult to analyze the test, therefore it was decided that the tests should be paused and subsequently continued the next morning. The total time of the test was around 30 hours and the maximum load was 87.3 kPa when the embankment reached failure.

Table 4.6: *Calculation steps*

Step	Description
1	Consolidation of the initial geometry (11 years)
2	Old fill is applied and consolidated (11 years)
3	Parts of the old fill is dug out and a ditch is built (5.5 years)
4	Construction of the embankment (2 months)
5	Weight representing the containers on top of the embankment is applied (1 hour)
6-42	Load applied and resting phase (tot. 28.6 hours)
43-48	Consolidation phases until failure (tot. 19.8 hours)

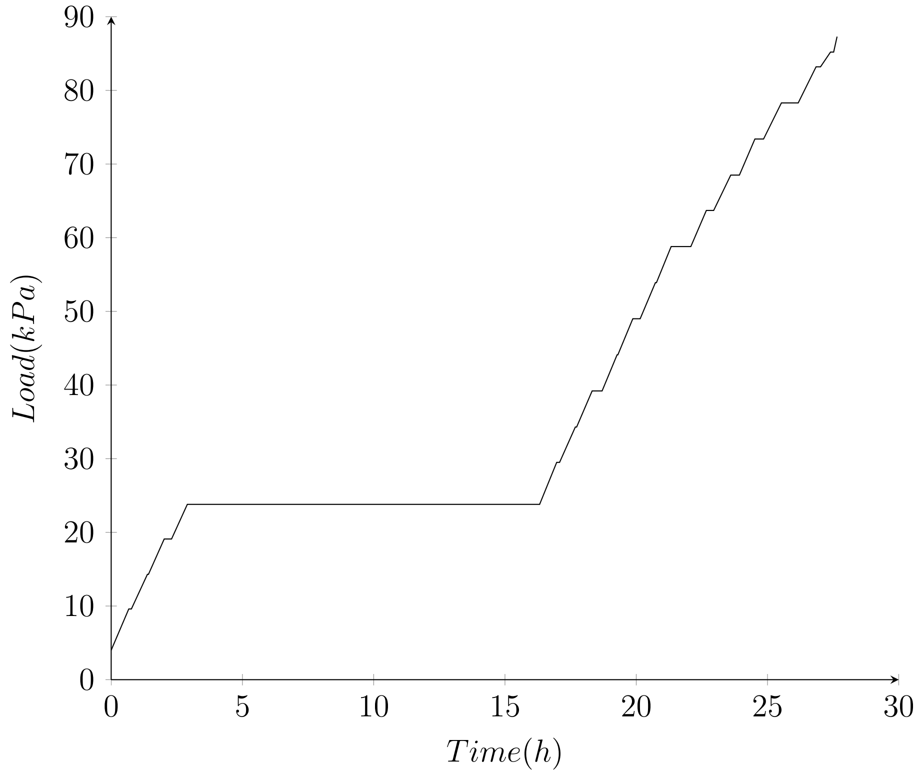

Figure 4.6: *Loading steps for the Perniö embankment failure test.*

4.6 Failure definitions

When analysing failure in Plaxis, certain guidelines needed to be set. The definition of failure was set to be at the point where large deformations occurred in a short time period after the model had been consolidated after a long time period. This could also be defined as the point where the deformations start to have a positive acceleration after a time of negative acceleration. In some cases the model reached its limit when the simulation could not be calculated further, meaning that the calculations failed after being consolidated. This was not defined as the failure of the model, but the time directly before failure.

4.7 Possible scenarios

In addition to the Perniö embankment failure test, two possible scenarios were simulated. The scenarios were a train standing still on the tracks of the embankment for a long time period. In the first simulation, the weight of the train is representative of the safety factor of 1.3 in relation to the failure load of 87.3kPa. The load of the train was therefore set to 55kPa. The second load was set to the load between 55kPa and the failure load 87.3kPa. The second simulation was therefore set to 71kPa.
The load was applied directly after the consolidation of the embankment. After this, time steps were applied in the simulation. The time periods were:

Step	Description
1	Consolidation of the initial geometry (11 years)
2	Old fill is applied and consolidated (11 years)
3	Parts of the old fill is dug out and a ditch is built (5.5 years)
4	Construction of the embankment (2 months)
5	10 hours consolidation
6	4 days consolidation
7	42 days consolidation
8	1.1 year consolidation
9	11.4 years consolidation
10	22.8 years consolidation
11	34.2 years consolidation
Tot	70 years consolidation

4.8 Measurement instrumentation

To compare with the measured displacements and pore pressures, measurement nodes were placed in the model. Figure 4.7 shows a cross-section of the embankment where the numbered blue circles represent the pore pressure measurement nodes, and the vertical grey lines represent the inclinometers. Node 1-5 at height 3.9m, 4.4m, 4.9m, 5.2m, and 5.4m are placed straight under the embankment. The heights are described as meters above sea level. Node 6-9 at height 2.1m, 2.7m, 3.3m, and 4m at the toe of the embankment. Node 10-12 are placed 6.7 horizontal meters from the embankment with heights at 3.2m, 3.9m and 4.6m, and nodes 13-15 are placed under the ditch with heights at 2.6m, 3.14m, 4.2m, and 4.8m. The three vertical lines represent the inclinometers which measure the lateral displacements. The inclinometers are placed in the gap between the three cars in the experiment, and in the model, these are placed between the embankment and the ditch with a horizontal spacing of 3.6m, 7m, and 10m from the centre of the embankment.

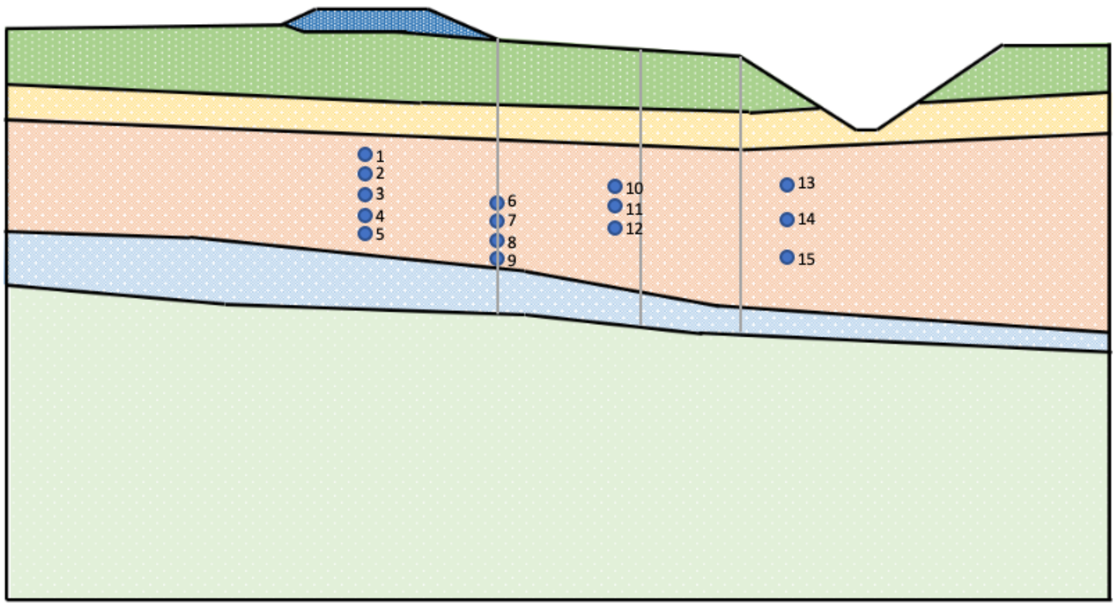

Figure 4.7: *Placement of measurement instrument in Plaxis model.*

5

Results and discussion

In the result and discussion chapter, the data retrieved from the simulations in Plaxis are presented and compared with the measurement data retrieved from the real performed embankment failure test. In geotechnics and also in this thesis, downwards pressure is described as negative pressure. The results are divided into different parts with a discussion included. The initial conditions are presented, where the state of the model before any load has been applied is analysed. The displacements from the simulated failure test from different points of view are presented. The pore pressures during the test, safety analysis to show the sensitivity of the model is analysed and the two alternative scenarios are presented where the deformations and pore pressures are analysed.

5.1 Initial conditions

Before any load was applied on top of the embankment, the initial conditions were determined. To have reliable results the soil was consolidated in the initial model. This to decrease the excess pore pressures after adding the new fill. The deformations from the consolidation were reset, before applying a load on top of the embankment. This made the soil parameters representative for a long time of consolidation while the geometry was not affected.
Figure 5.1 shows the initial geometry before any load was applied on top of the embankment. In the ditch, the Figure shows that water pressures are building up in the bottom of the ditch presented as green arrows. This happens because the groundwater table is higher than the bottom of the ditch.

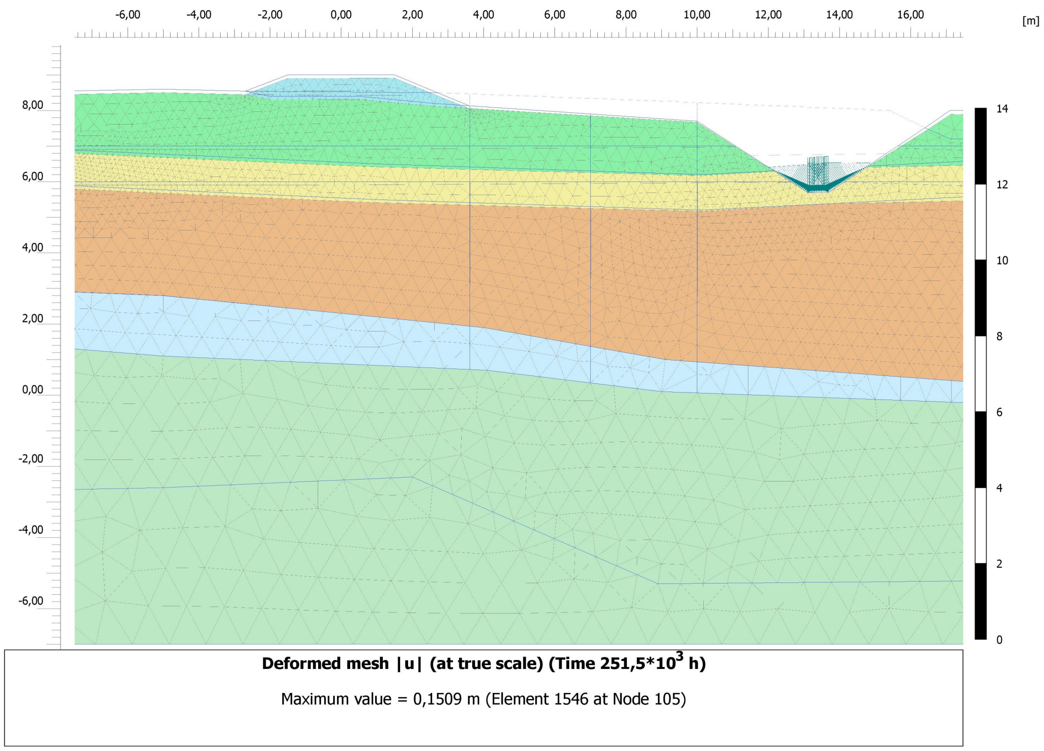

Figure 5.1: *Deformations before loading*

Figure 5.2 shows the excess pore pressures at the time before the load was applied. It can be seen that the largest pore pressures were directly under the embankment in clay 1. However, these pore pressures were relatively small. The maximum excess pore pressure predicted was 3.4 kPa. To the right of the ditch, some excess pore pressures can be seen as well. This due to the load from the new fill layer added in the construction phase of the ditch.

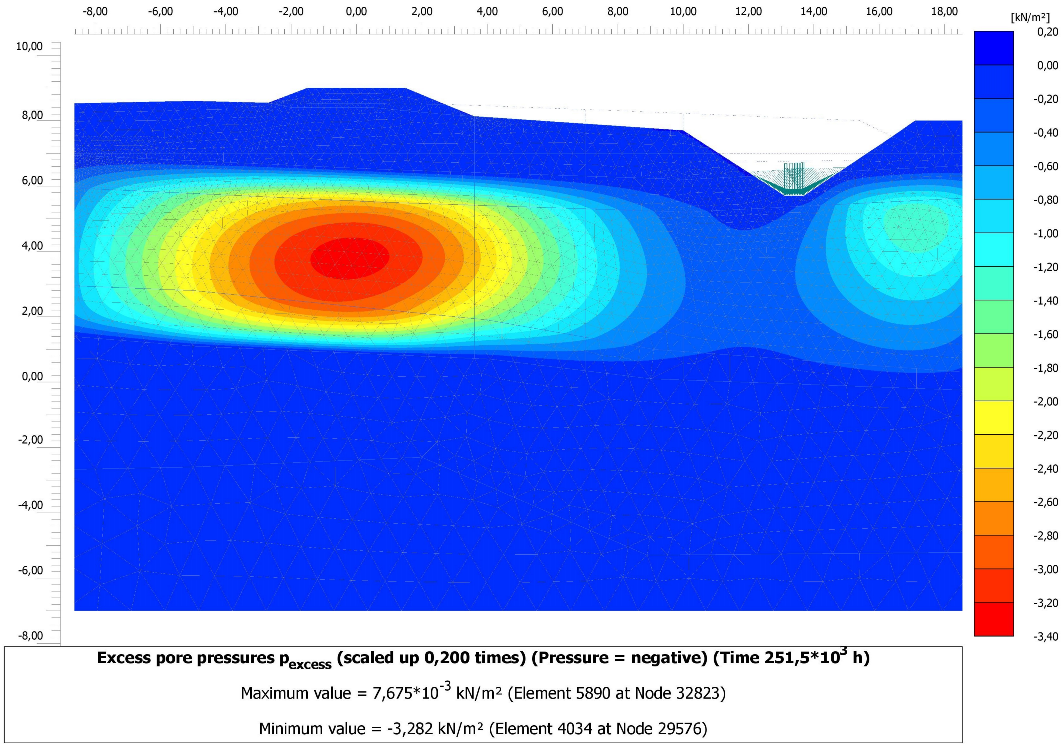

Figure 5.2: *Excess pore pressures before loading of embankment*

5.2 Displacements

The displacements of the embankment were analysed by looking at deformations in the last loading step, before failure and at the point of failure. The time for the failure step was 0.1 hours. By looking at the deformed mesh for each of these steps, an overview of how the deformations occurred can be seen. The total displacement tool is used to see where the displacements were largest and how the displacements were distributed. To see possible slip surfaces and how the displacements increased at the point of failure the incremental displacement tool was used.

The embankment was loaded with 87.3 kPa. The last load was applied after 28.6 hours. After this, the embankment let to consolidate and creep until it reached failure. The embankment reached failure after consolidating for 19,8 hours after the last loading step. The displacements are presented in the Figures 5.3 - 5.12.

5.2.1 Deformed mesh

In Figure 5.3 the deformations after the last loading step are presented. The deformations are mainly by the embankment. The deformations reach clay layer 1. It can be noted that the model to some extent has consolidated and crept from the weight of the new fill, and not only from the load on top of the embankment.

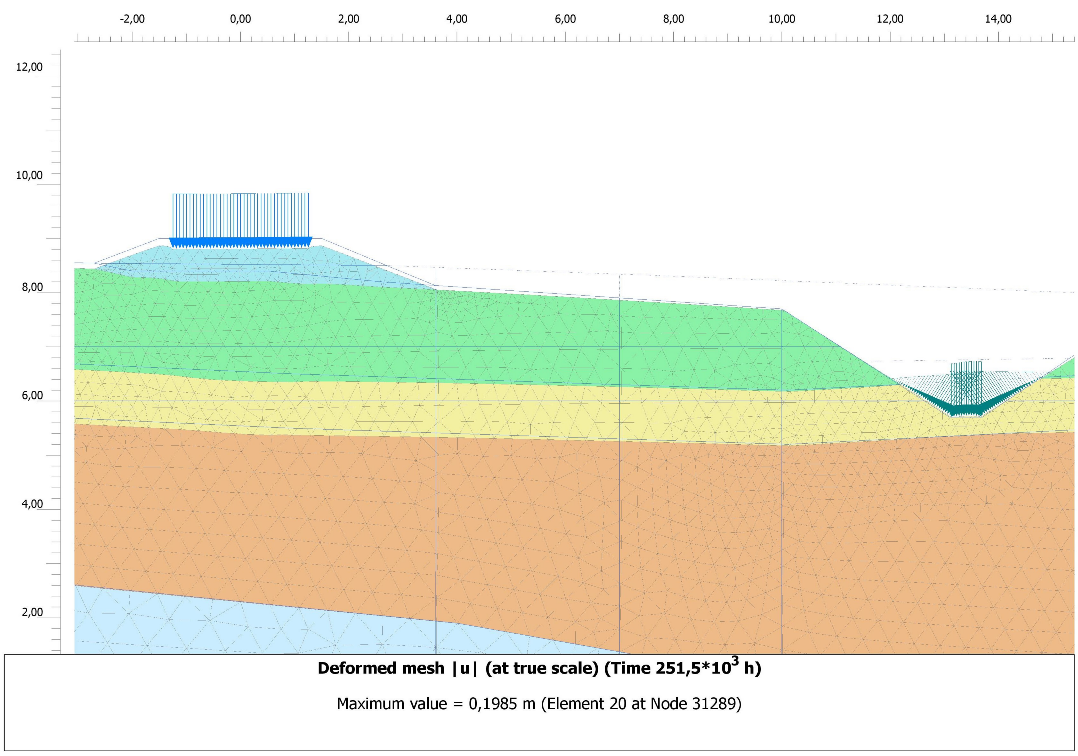

Figure 5.3: *Deformations at last loading step*

At the point of failure, the embankment has deformed so much that a slip surface is initiated. This is shown as a rounded deformation from the embankment towards the ditch and can be seen in Figure 5.4. The embankment has deformed in a vertical direction, and at the ditch, there are horizontal displacements at the left side of the ditch. This since the soil pushed by the embankment load towards the ditch. The displacements follow a distinct rounded line that reaches +3m of the model in Clay 1.

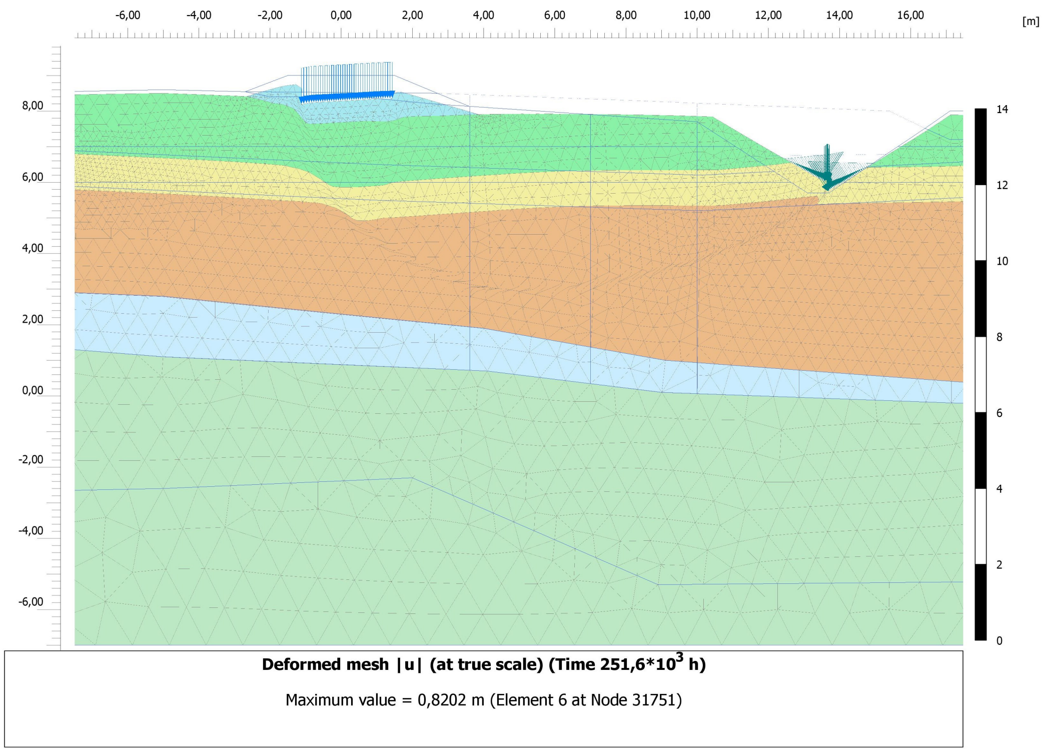

Figure 5.4: *Deformations at failure*

5.2.2 Total displacements

Figure 5.5 shows the total displacements after the last loading step. In the mesh, it can be seen that most of the predicted displacements are located directly under the embankment. The maximum displacements reach 0.2m and are located under the embankment. No signs of failure can be seen in this mesh. The deformations outside of the embankment are due to the soil following the vertical displacements of the embankment and these deformations, therefore, seem to decrease further away from the embankment.

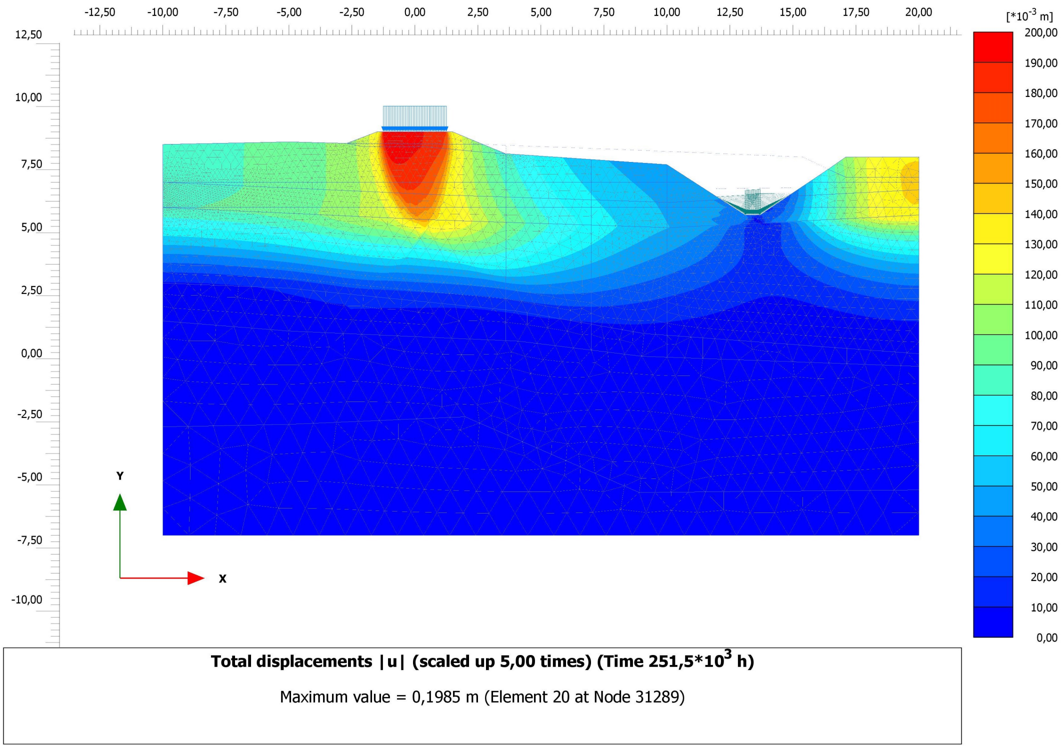

Figure 5.5: *Total displacements last loading step*

Figure 5.6 shows the predicted displacements before failure. The mesh shows that the majority of the larger displacements were directly under the embankment. The largest displacements were on the left side of the embankment. The maximum displacements reached 0.45m. It can be seen that most of the displacements are distributed between the embankment and the ditch.

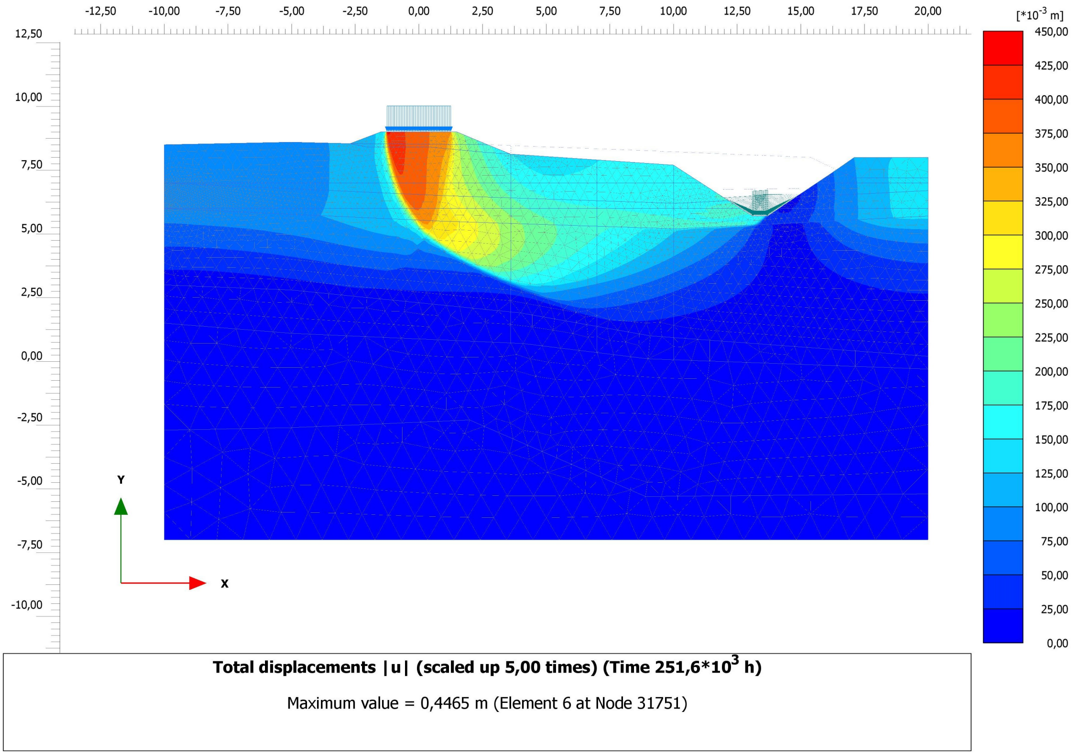

Figure 5.6: *Total displacements before failure*

Figure 5.7 shows the predicted total displacements at the point of failure. The mesh shows a larger difference in the displacements than directly before failure shown in Figure 5.6. At the point of failure, the left side of the embankment has reached displacements of 0.85m. The displacements are located between the embankment and the ditch. It can be seen that the displacements towards the ditch are predicted to be larger than the displacements before failure. In Figure 5.7 the displacements follow a distinct circular line from the embankment towards the ditch. Directly to the right of the embankment a light blue section can be seen representing smaller deformations. An outcome from this could be that soil cracks appear at the surface in the real case scenario.

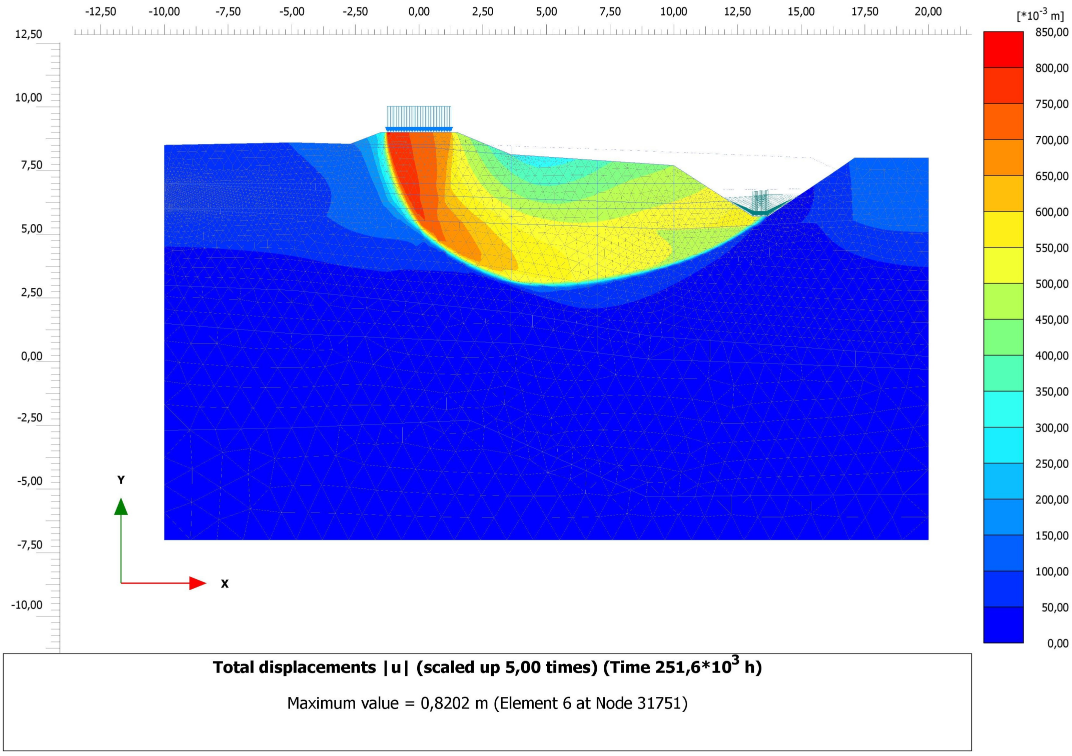

Figure 5.7: *Total displacements at failure*

5.2.3 Incremental displacements

Figure 5.8 shows the predicted incremental displacements at the last loading step. The time for this step was 0.13 hours. The mesh does not indicate a distinct slip surface. What can be seen is that the majority of the incremental displacements are between the embankment and the ditch. The largest incremental displacements are on the left side of the embankment.

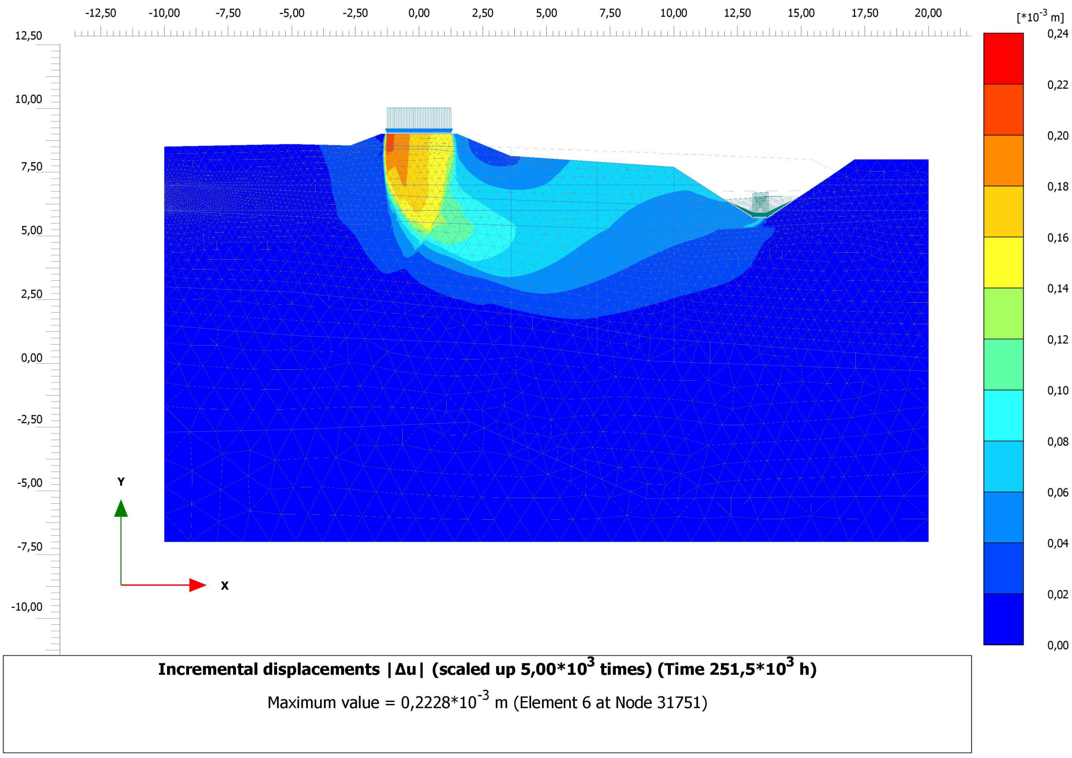

Figure 5.8: *Incremental displacements at last loading step (0,13 hours)*

In Figure 5.9 the incremental displacements before failure indicate that a slip surface has formed. The incremental displacements are between the embankment and the ditch. The largest incremental deformations are directly under the embankment, these deformations clearly follow the slip surface. At this stage, the major displacements reach about halfway along the slip surface. After this the deformations mainly go upwards towards the left side of the ditch, this can be seen as a yellow section.

In Figure 5.10 the incremental displacements show a distinct slip surface and how the deformations clearly follow this slip surface. The incremental displacements are larger than the incremental displacements before the failure from Figure 5.8. At this point, the incremental displacements reach the ditch towards the bottom of the ditch in comparison to the incremental displacements from Figure 5.9 that were towards the upper section of the ditch. The time for the failure step was 0.1 hours.

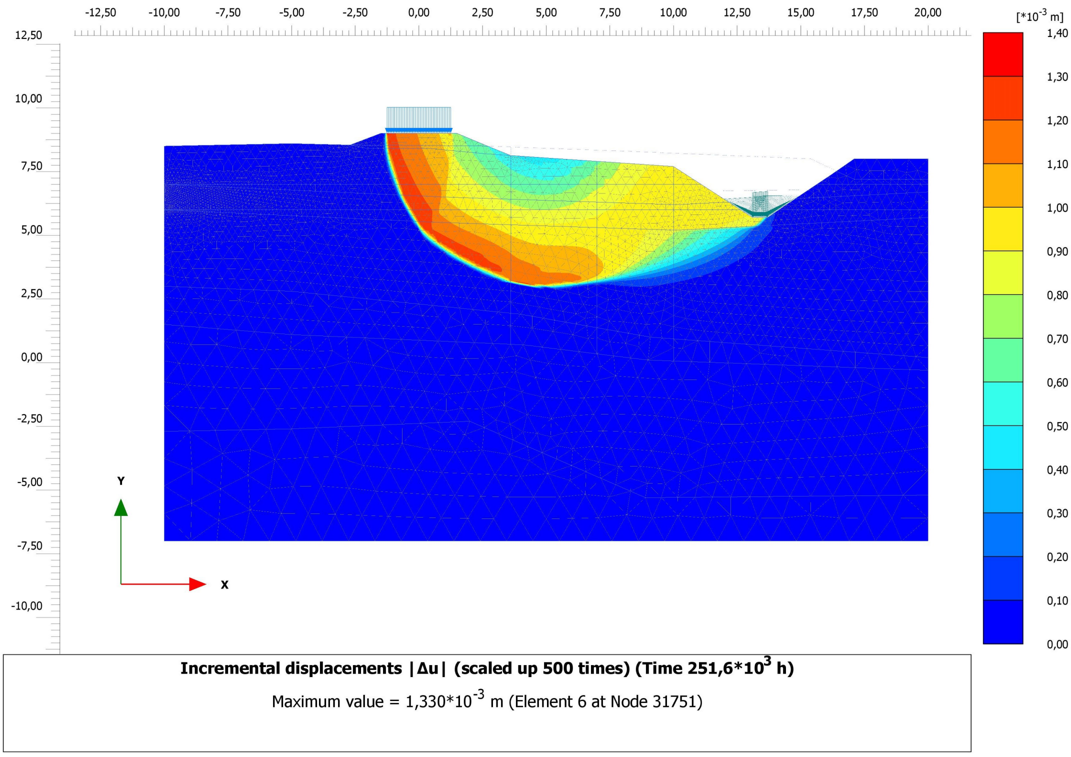

Figure 5.9: *Incremental displacements before failure (0.3 hours)*

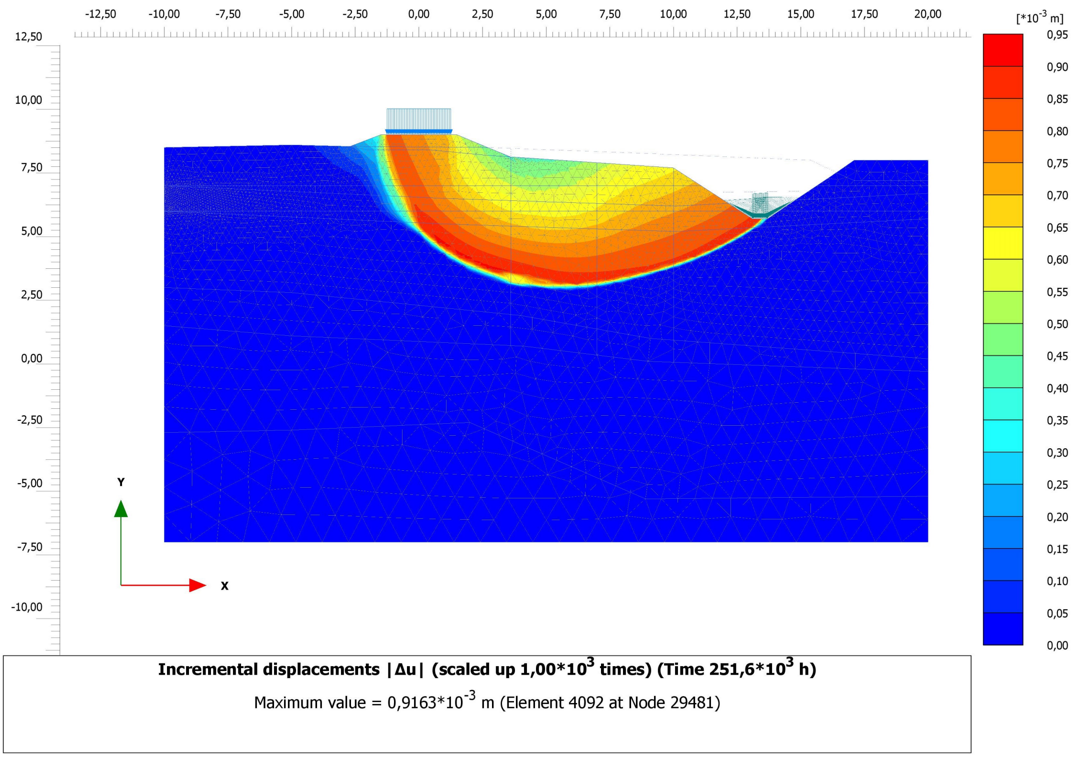

Figure 5.10: *Incremental displacements at failure (0.1 hours)*

5.2.4 Horizontal displacements

In Figure 5.11 - 5.13 the predicted horizontal displacements are compared with the measured horizontal displacements in situ made by Lethonen (2011). The horizontal displacements were measured at three points with the help of inclinometers. The legend shows the time from the first loading step and corresponds to the time for the measurement data from the site. The placement of these measurement points is presented in Figure 4.7. The results show that the horizontal displacements were larger closer to the embankment and at a depth of -3.5 m from the ground surface at the beginning of the first clay layer. The maximum horizontal displacement reached 0,21 meter. Closer to the ditch the horizontal displacements decreased, however, the displacements changed in terms of how they were distributed over the depth.

Figure 5.11 show the measured and predicted horizontal displacements 3.6m from the embankment, Figure 5.12 show the measured and predicted horizontal displacements 7m from the embankment and Figure 5.13 show the measured and predicted horizontal displacements 10m from the embankment. The yellow lines in the bottom graphs are the predicted measurements that correspond to the blue lines in the top graphs if considering time. The magnitude of the displacement at this time is similar, except for the displacements 10 meters from the embankment that differs. When comparing the predicted horizontal displacements at failure from the simulation in Plaxis the results differ in magnitude. The predicted displacements before failure are more than twice as large as the measured displacements before failure at the site. However, the displacements are similar in the way they are distributed over the depth. An explanation of the difference in the magnitude of the displacements could be attributed to the stiffness of the inclinometer tubes that are not accounted for in the Plaxis analyses. Also, when looking at the displacements predicted in Plaxis, the containers would have fallen before the point of failure according to Plaxis due to gravity and instability of the containers. This is an important aspect when looking at failure tests in Plaxis. Since the load is inserted as a line load and not as containers the failure mechanism is not identical. The real failure test was over when the containers fell over, while the simulated test finished when the ground reached its limit state.

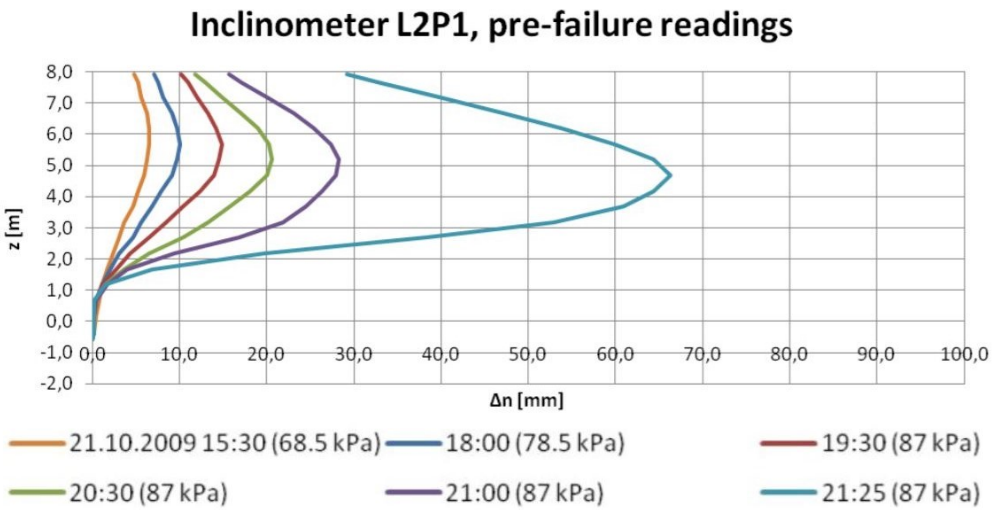

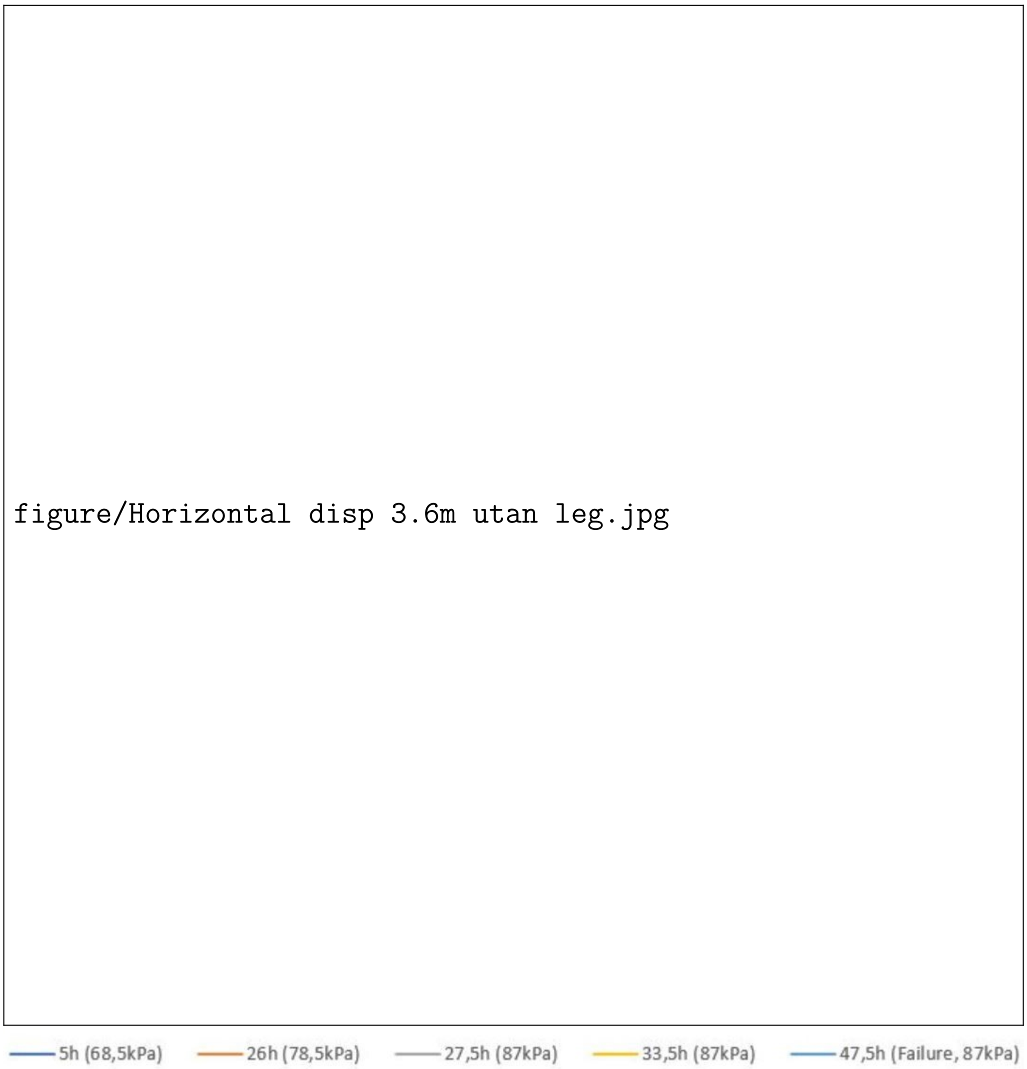

Figure 5.11: *Comparison of instrumental (Lethonen, 2011) and predicted measurements of horizontal displacements 3.6m from embankment*

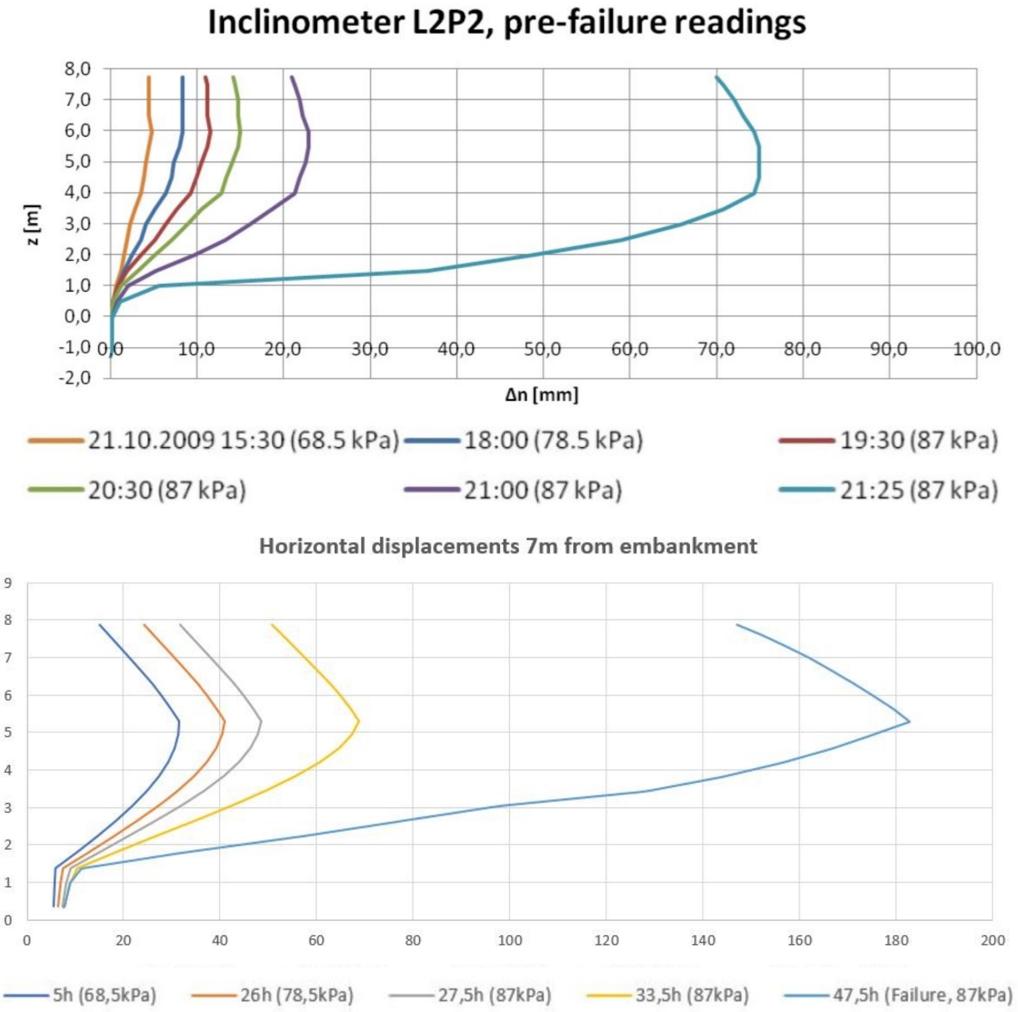

Figure 5.12: *Comparison of instrumental (Lethonen, 2011) and predicted measurements of horizontal displacements 7m from embankment*

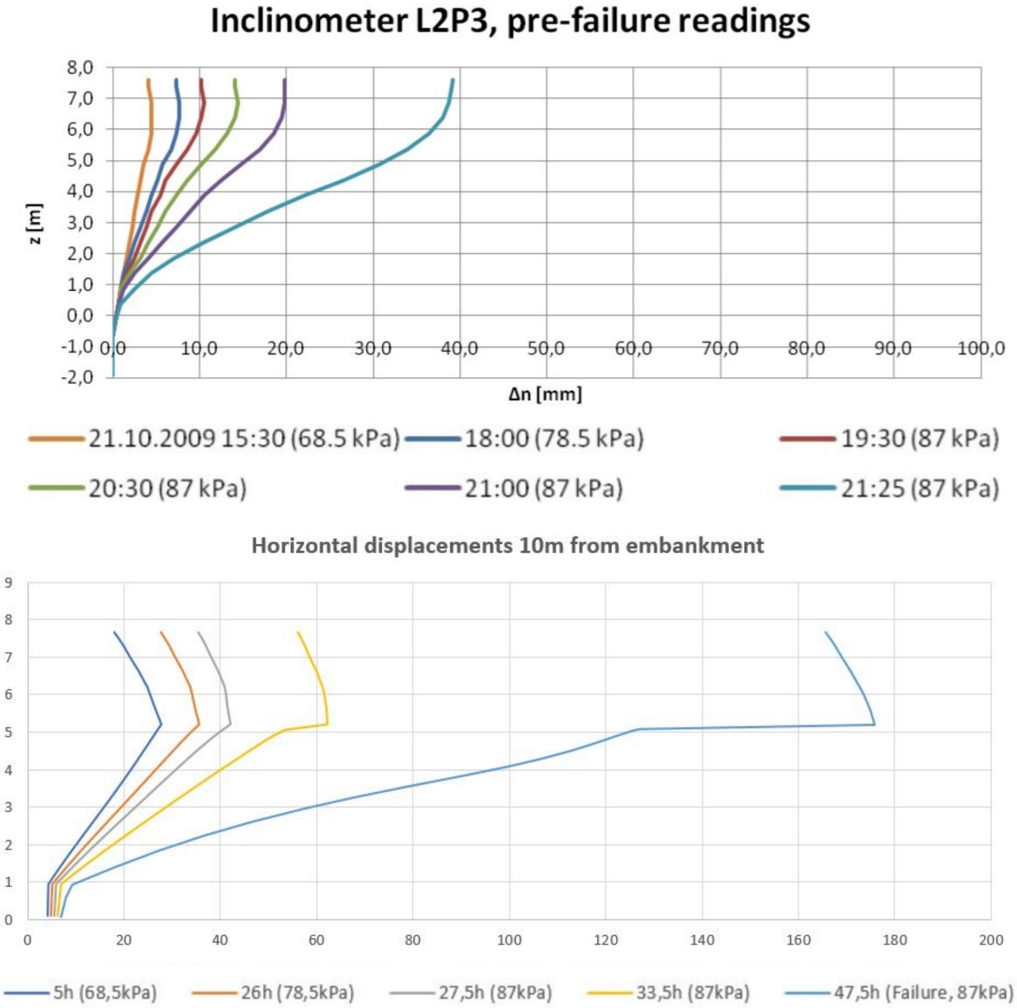

Figure 5.13: *Comparison of instrumental (Lethonen, 2011) and predicted measurements of horizontal displacements 10m from embankment*

The relation between the predicted vertical and horizontal displacements can be seen in Figure 5.14. The measurement point was centered under the embankment. The graph shows the ratio between the horizontal and vertical displacements at the beginning of the first clay layer (+6m) under the embankment. The vertical displacements had a larger start value since some consolidation has occurred before the displacements from the applied load. However, the deformations follow each other similarly. It can be seen that the displacements are increasing both vertically and horizontally after the last loading step at 28 hours. At the point of failure, there are large deformations both vertically and horizontally. The predictions indicate deformations outside of the yield surface. This can be seen as the section where the displacements start to increase linearly after about 16 hours. At this point, the deformations therefore are predicted to be irrecoverable.

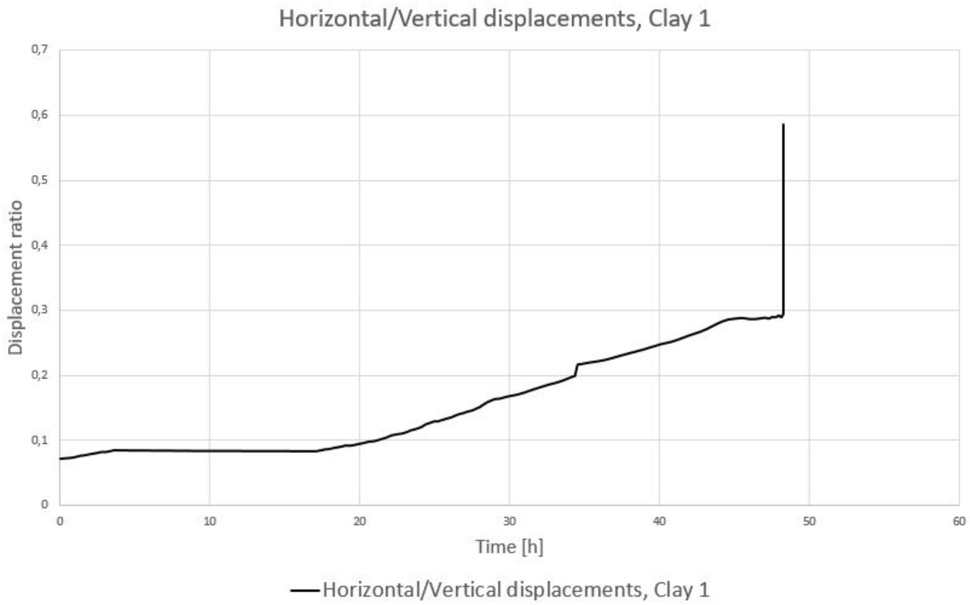

Figure 5.14: *Vertical and horizontal displacements (+6m and +8m)*

5.3 Pore pressures

During the loading of the embankment, excess pore pressures developed. When looking at the excess pore pressures it is seen in Figure 5.15 that at the last loading step the pore pressures were largest straight under the embankment, in the top of clay layer 1. Important to highlight is that in geotechnics and in Plaxis downwards pressure is described as negative in contrast to the structure. Due to the groundwater level following the top surface of the dry crust, it is reasonable to not have pore pressures of concern in the layers above.

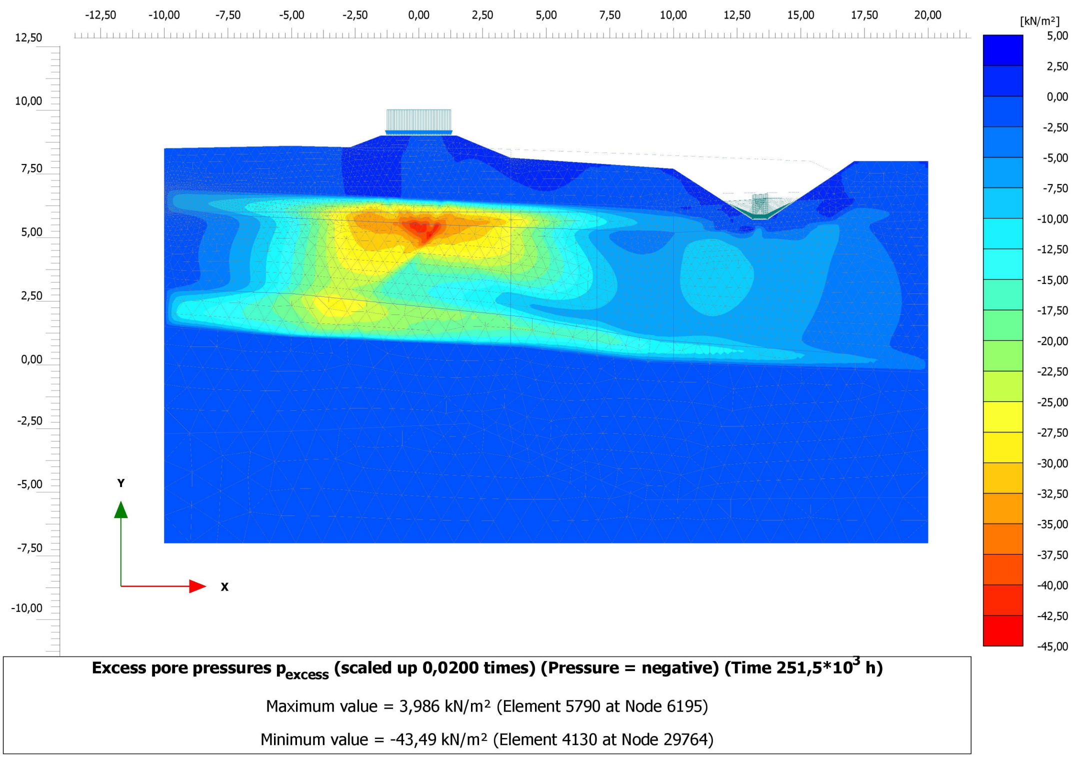

Figure 5.15: *Excess pore pressures at last loading step*

Figure 5.16 shows the excess pore pressure just before failure occurs. Here it can be seen that the pore pressures have moved and almost coincide with the slip surface seen in Figure 5.9. The pore pressures are connected to the compression, creep, and the permeability of the soil. The low permeability of the clay prevents dissipation of the excess pore pressure, which will continue to develop due to creep with the increasing load on top of the embankment.

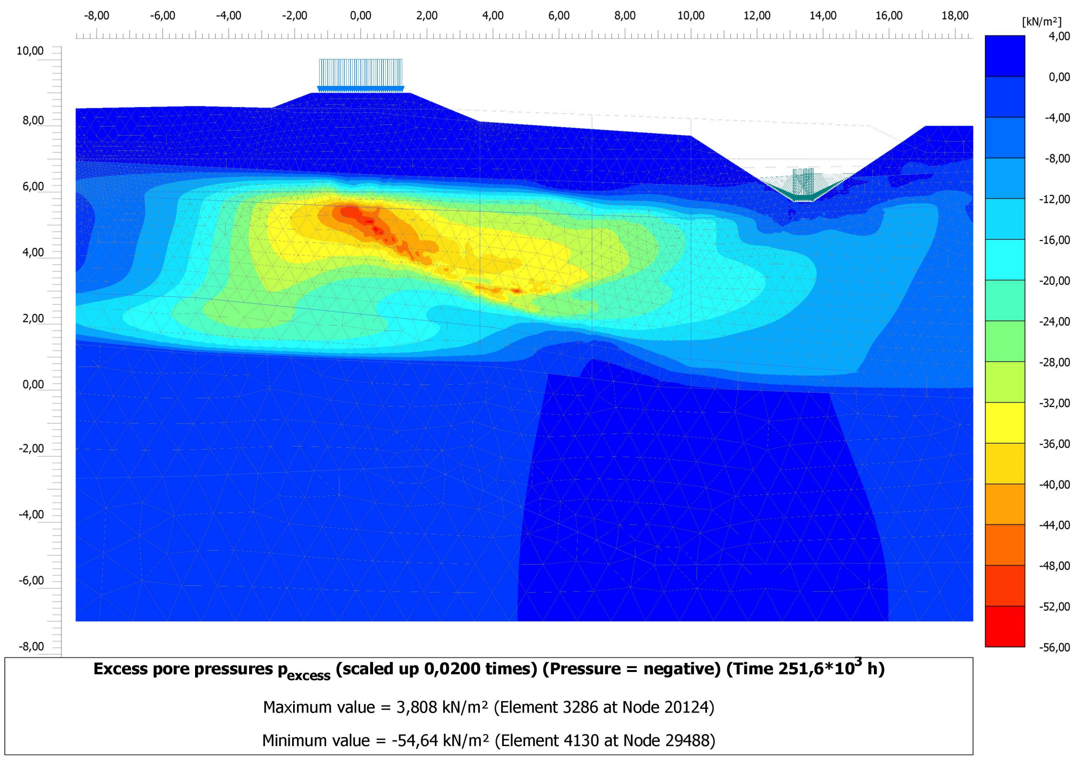

Figure 5.16: *Excess pore pressures before failure*

The pore pressures in the permeable fill layers have an opposite value compared to the clay layers. These positive pore pressures are an indication of increasing the stability of the embankment.

At the point of failure seen in Figure 5.17, the pore pressures changed drastically. This is an indication that failure actually was reached. When the built-up pressures rapidly decrease it means that a lot of the forces contributing to the stability of the soil are taken away. Comparing to the pore pressures before failure some areas at the failure point have positive pore pressures. This is an indication of large visco-plastic deformations.

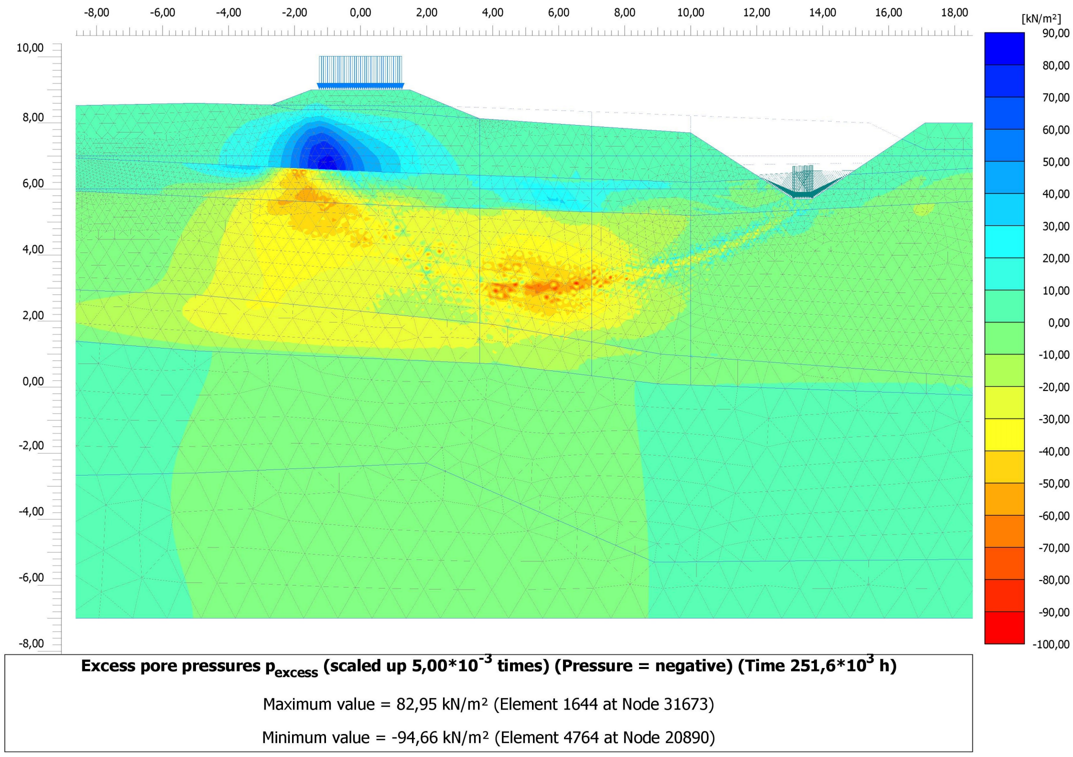

Figure 5.17: *Excess pore pressures at failure*

Figure 5.18, 5.20, 5.22, and 5.24 show the pore pressures over time at four measurement points from the Plaxis model. The pore pressures are presented with different depths shown in section 4.6 and Figure 4.7. The measurement began at the first loading step and continued during loading and until failure. The results are similar to the results measured and analysed by Lethonen, 2011. The predicted pore pressures from the Plaxis model are compared with the measured pore pressure values at the site for all measurement points. The measured values performed by Lethonen, 2011 starts 10 hours after the loading started (T=10h).

Under the embankment in Figure 5.18 it is seen that the pore pressures increased almost linearly during loading and where the pore pressure start to abate are during consolidation and creep. The increase of pore pressures has negative values due to geotechnical standards in Plaxis. Figure 5.19 shows the pore pressures measured from time T=10h and starts at 15-25 kPa, increasing to between 40 and 45 kPa which is in line with the modelled values at the same time with a difference of 5-10 kPa. The pore pressures are continuously increasing until the time at failure which also can be seen in Figure 5.18- 5.24.

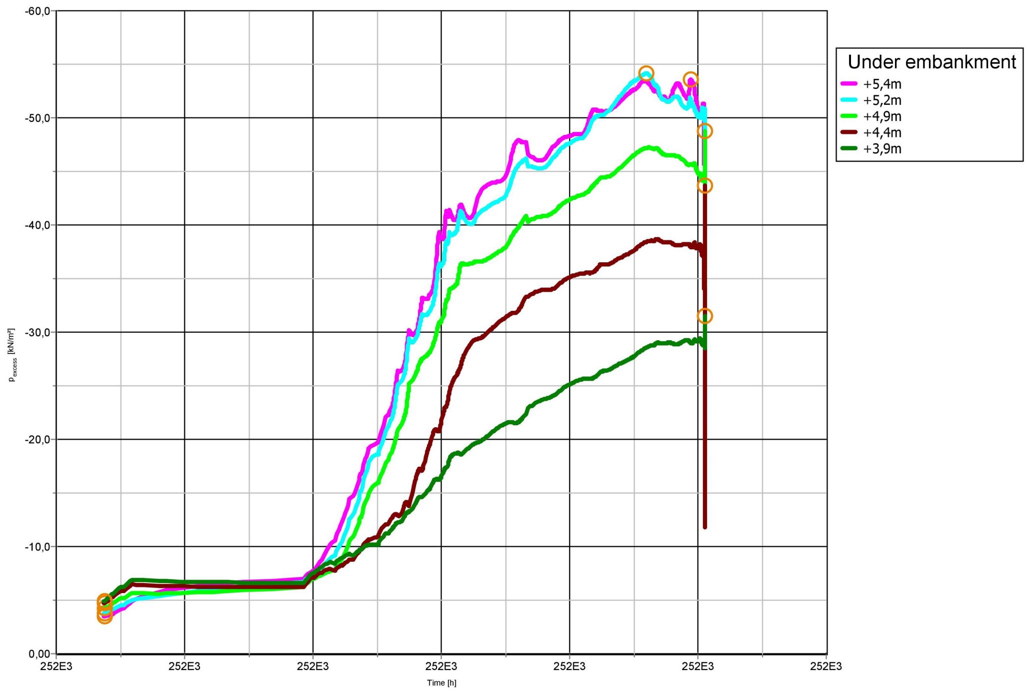

Figure 5.18: *Predicted excess pore pressures under embankment*

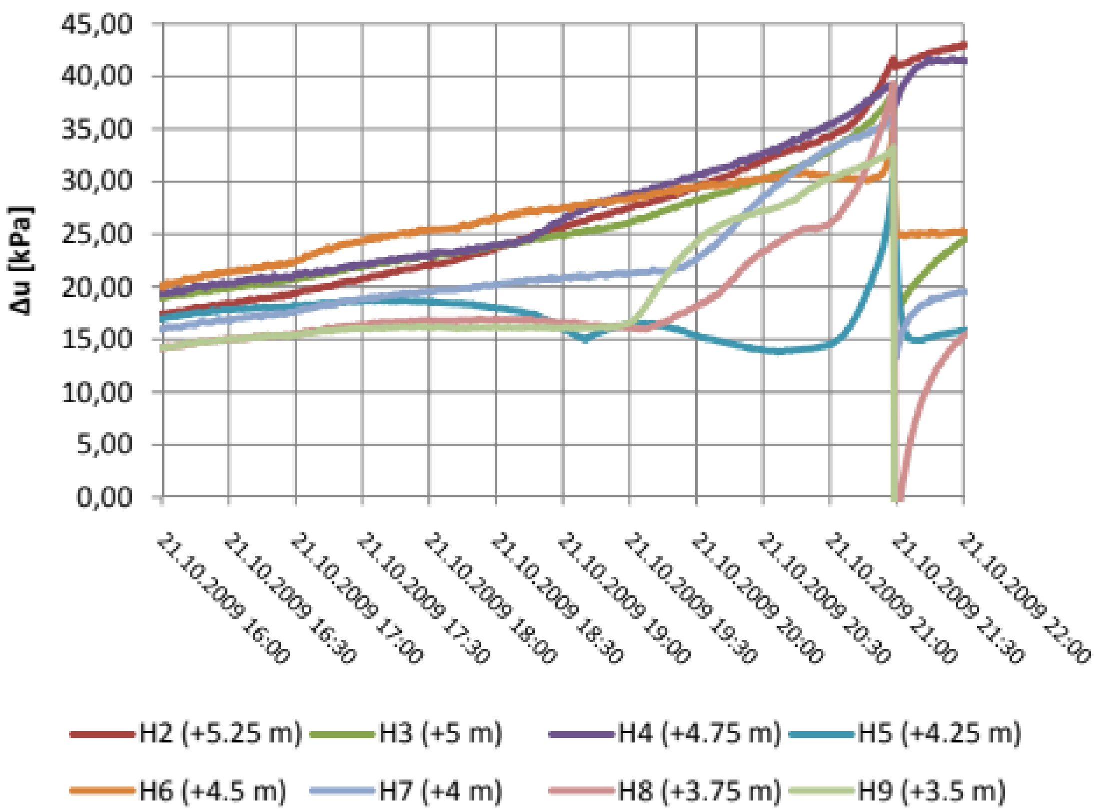

Figure 5.19: *Measured excess pore pressures under embankment (Lethonen, 2011)*

Figure 5.20-5.24 shows the pore pressures over time under the embankment toe, 6.7 meters from the centre of the embankment, and under the ditch.
The pore pressures at the embankment toe are higher in measured points, closer to the surface which is similar to the results shown in Figure 5.2-5.16. The deeper measurement point shows a lower pore pressure and can be connected where the failure takes place in the soil.

Figure 5.22 shows the predicted pore pressures 6.7m from the embankment and Figure 5.23 shows the predicted pore pressures under the ditch. The graphs show that the predicted pore pressures have a lower incremental slope compared to the measurement points closer to the embankment, caused by lower pore pressures. The measurement points further away from the embankment are exposed to a lower load which is the reason for the lower pore pressures. The predicted pore pressure values presented in Figure 5.22 and 5.23 are similar to the pore pressures measured at the site which are shown in Figure 5.24 when comparing from T=10h. Figure 5.24 shows the combined results from the measurement points 6.7m from the embankment and under the ditch. Line H19-H24 corresponds to the measurement point 6.7m from the embankment and line H25-H31 corresponds to the measurement point under the ditch.

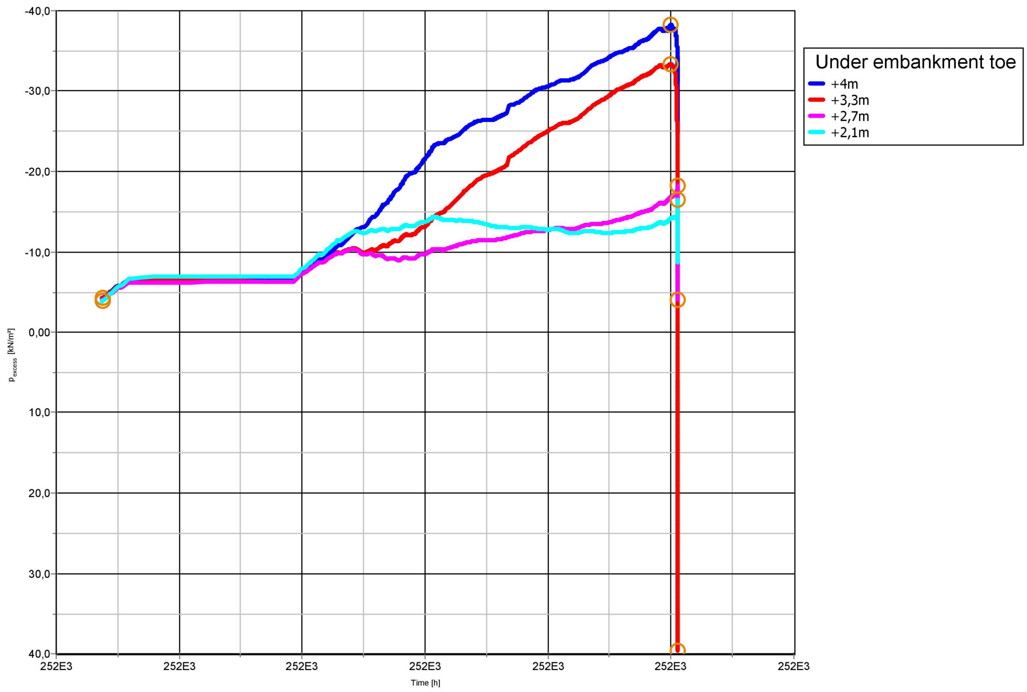

Figure 5.20: *Predicted excess pore pressures under embankment toe*

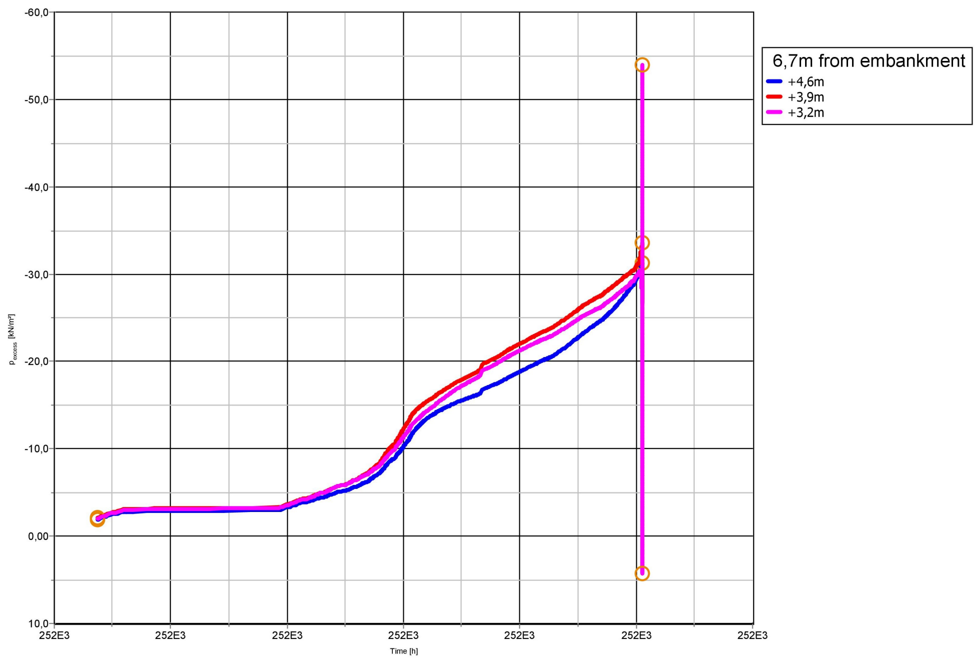

Figure 5.22: *Predicted excess pore pressures 6,7m from embankment*

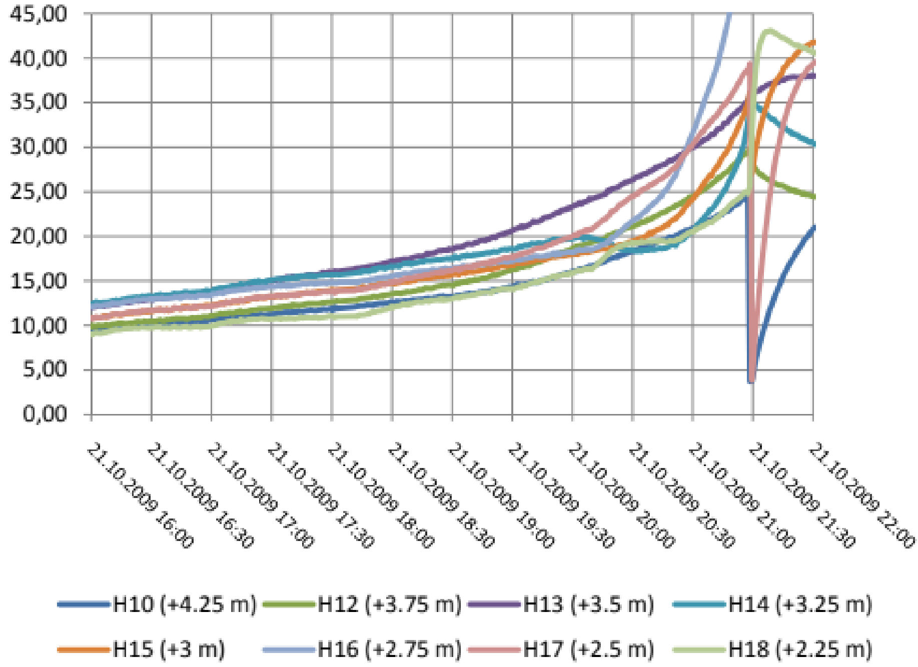

Figure 5.21: *Measured excess pore pressures under embankment toe (Lethonen, 2011)*

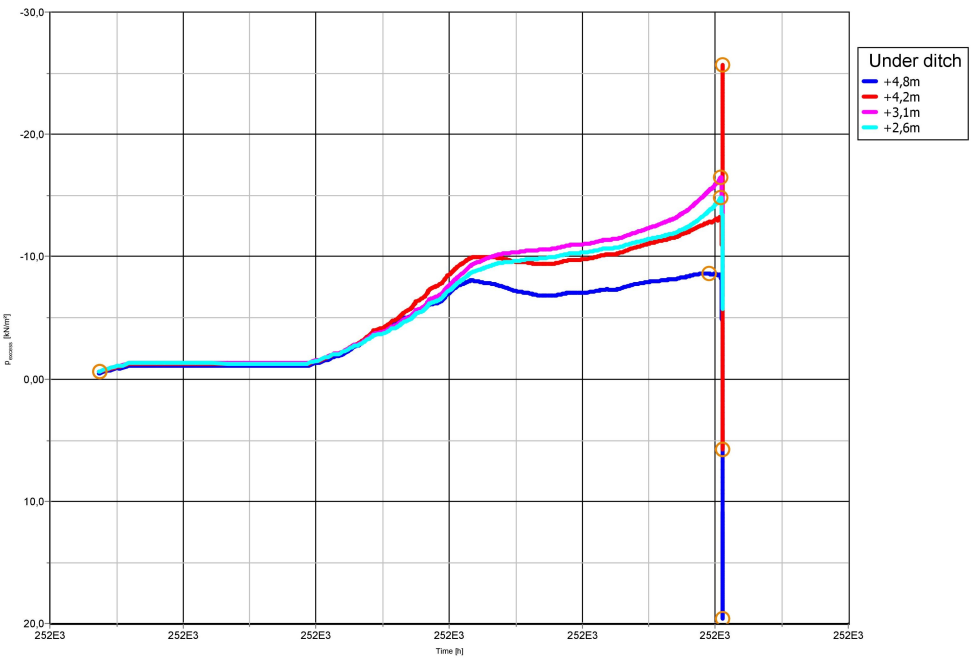

Figure 5.23: *Predicted excess pore pressures under ditch*

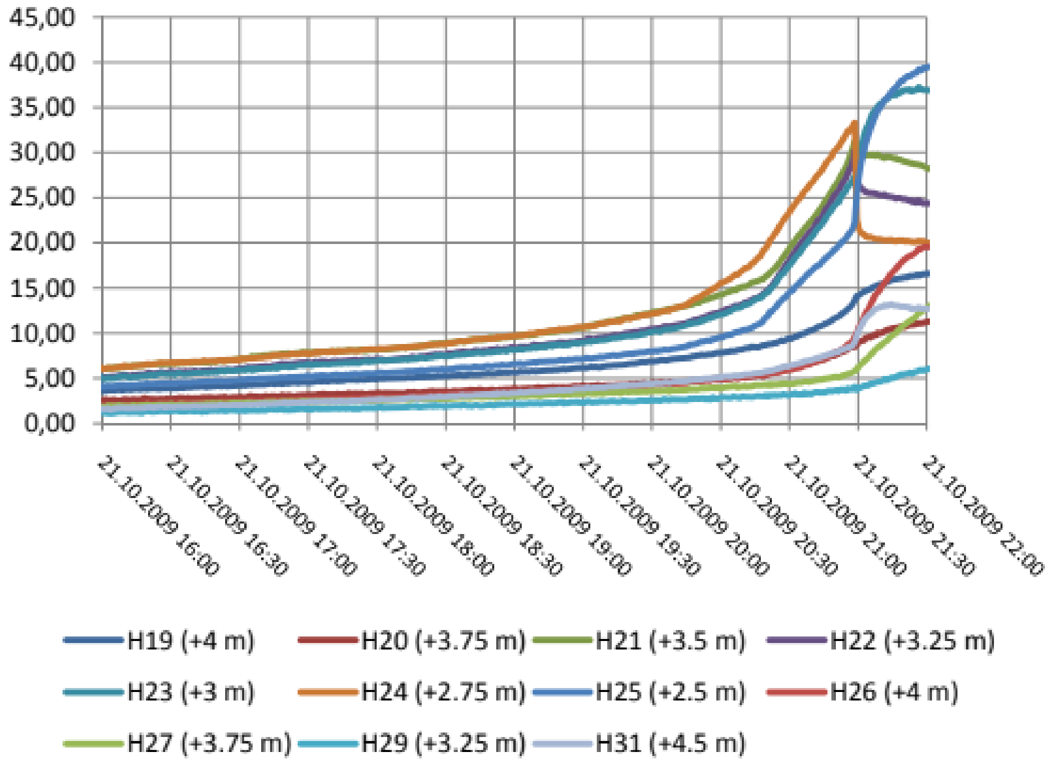

Figure 5.24: *Measured excess pore pressures 6.7m from the embankment and under the ditch (H19-H24: 6.7m from embankment, H25-H31: Under the ditch) (Lethonen, 2011)*

5.4 Sensitivity analysis

To study the reliability of the model a sensitivity analysis was made by varying the over consolidation. This was made by adding or subtracting 10kPa and 3 kPa, respectively, of POP in the Clay layer 1 separately. This to determine how sensitive the results of the model were. The models were compared in the stage right before failure. This since deformations can differ at the point of failure, and because the finite element method is not optimized to simulate the failure of soils. The comparison of the simulations with different POP is summarised in Table 5.1.

Table 5.1: *Comparison between different POPs.*

POP [kPa]	Maximum displacement [mm]	Time before failure [h]	Comment
24-19 (+10)	256	1.4	
17-12 (+3)	420	12.25	
14-9	450	19.9	Reference model
11-6 (-3)	622	13.25	
4-1 (-10)	550	N/A	Did not reach failure

In the model with +10kPa of POP the results differed in terms of how the model deformed as can be seen in the first picture in fig 5.14. The results show that the deformations are mainly in the top layers and reach 0.5 meters under the dry crust. The magnitude of the predicted deformations is smaller than predicted by the reference model, as can be seen in the first picture in fig 5.13 and the maximum displacement is 256mm right before failure. The model reached failure after 1.4 hours and was thus much more instantaneous.

When adding 3 kPa of POP to the model the simulation did reach failure after being consolidated for 14.5 hours after the last loading step. In fig 5.14 it can be seen that the deformations were similar to the original case. However, the slip surface did not reach the same depth as the reference model. The magnitude of deformations was similar to the original model with a maximum displacement of 420mm.

When subtracting 3 kPa of POP to the clay layer the model reached failure after 13.25 hours of consolidation and creep. The predicted deformations again differed from the original model. Compared to the reference model the displacements reached clay layer 2. The slip surface reached down to the section between Clay 1 and Clay 2.
The model with -10kPa of POP did not reach failure. The displacements did not show a clear slip surface, as can be seen in the last picture in fig 5.14. The maximum displacement reached 550mm after 20000 hours of consolidation.

In Figure 5.25 below the total deformations can be compared from the sensitivity analysis. The top left mesh shows +10kPa of POP, the top right mesh +3 kPa of POP, the original mesh is in the left-center, the mesh with -3 kPa of POP subtracted is in the right-center and the mesh with -10kPa of POP is at the bottom.

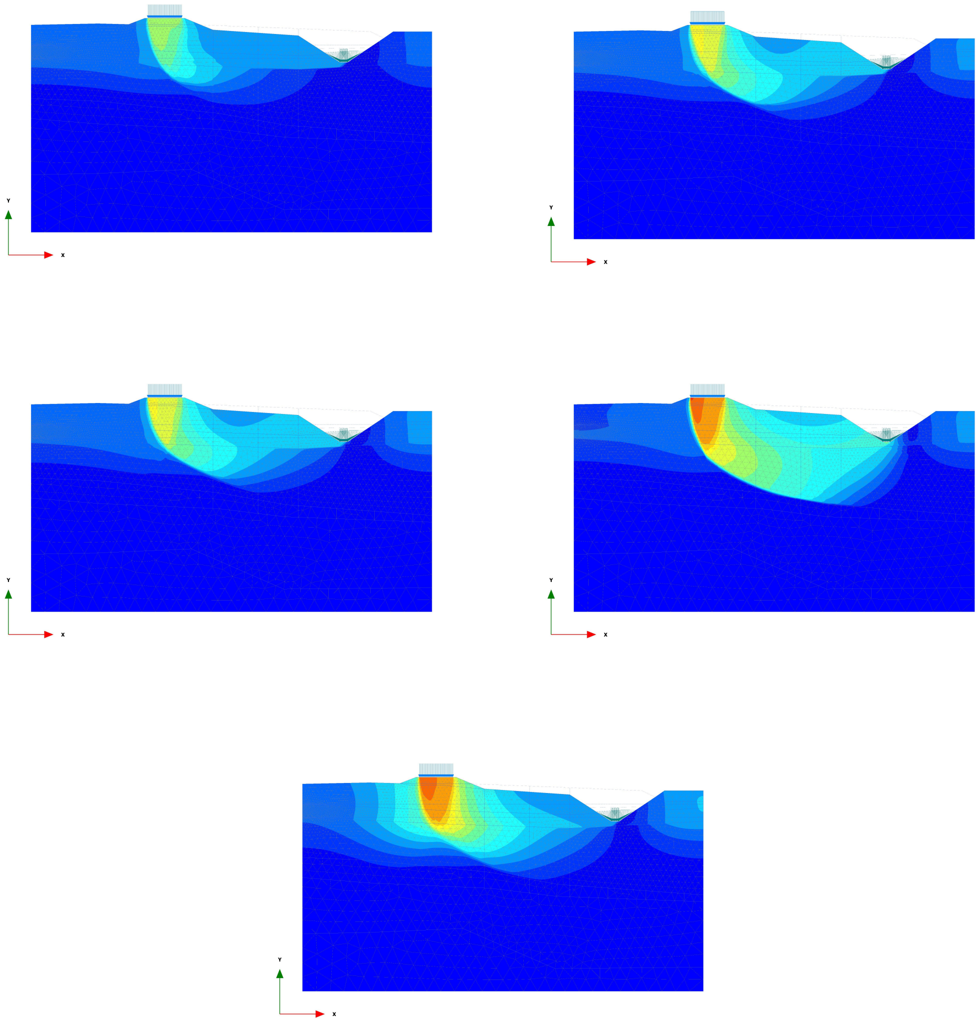

Figure 5.25: *Comparison of total deformations before failure in sensitivity analysis (+10 kPa POP, +3 kPa POP, original, -3 kPa POP, -10kPa POP)*

In Figure 5.26, the incremental displacements from the sensitivity analyses can be compared. These analyses give an indication of how the mode of deformations differs between the simulations. The top left mesh shows +10kPa of POP, the top right mesh +3 kPa of POP, the original mesh is in the left-center, the mesh with -3 kPa of POP subtracted is in the right-center and the mesh with -10kPa of POP is at the bottom.
The scenarios with higher and lower POP showed very different results compared to the reference model. A larger difference in POP resulted in a larger difference in results. However +/-3kPa of POP in a model is a relatively small change, and the

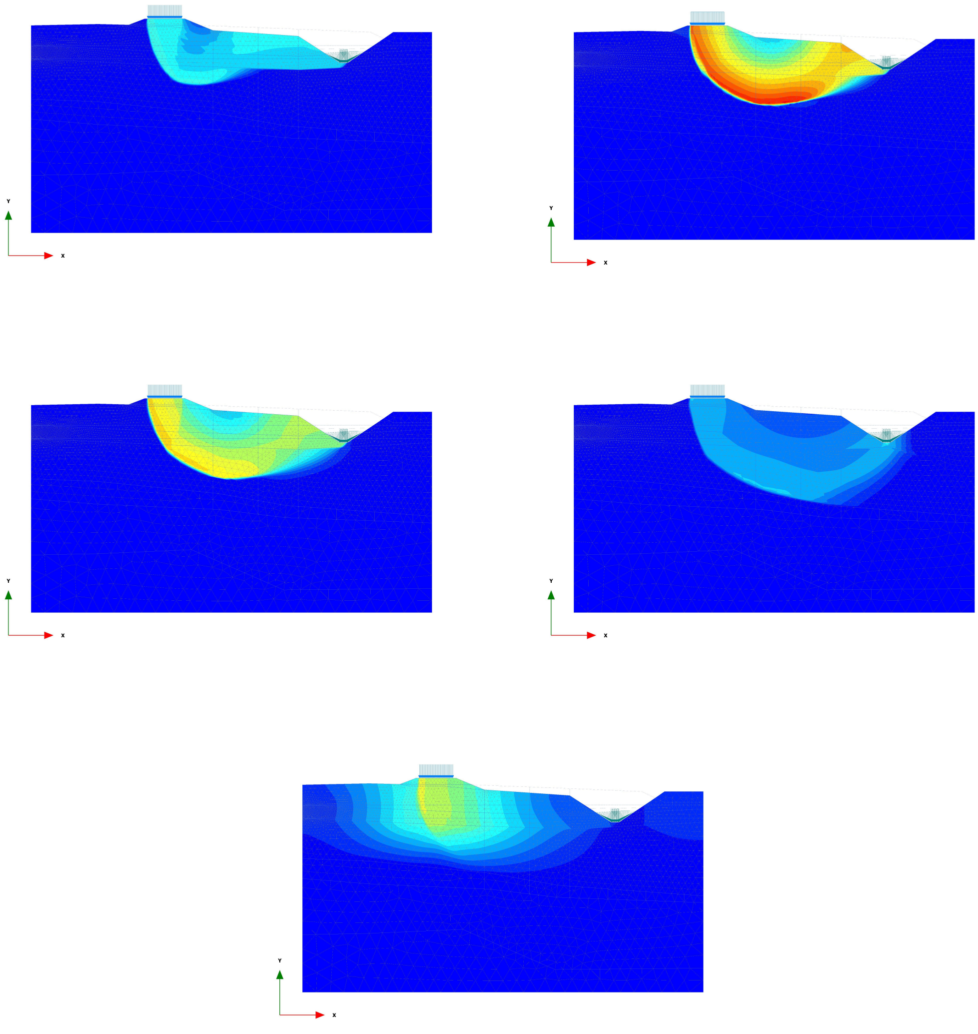

Figure 5.26: *Comparison of incremental deformations before failure in sensitivity analysis (+10 kPa POP, +3 kPa POP, original, -3 kPa POP, -10kPa POP)*

difference in the results demonstrated that creep models are very sensitive to the assumed pre-consolidation pressure.

5.5 Possible scenarios

In addition to the Perniö embankment failure test as it was made, two possible scenarios were simulated with the numerical model. The scenarios are a train standing still on the tracks of the embankment for a long time period with two different loads. The loads were 55 kPa and 71 kPa.

5.5.1 Train load, 55kPa

The results from the scenario with a constant load of 55 kPa for a long time period are presented below.

The scenario did not indicate a risk of large deformations. In figure 5.27 the deformed mesh did not show large visible deformations. The predicted displacements due to consolidation and creep seem to be rather uniform and follow the ground surface.

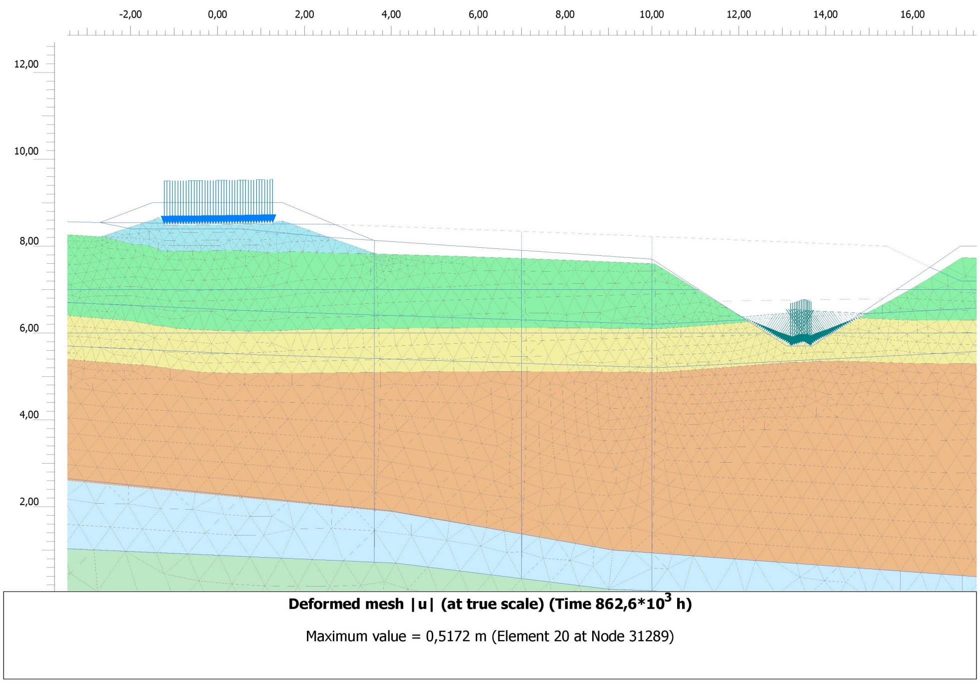

Figure 5.27: *Deformations from train load 55kPa after 70 years*

From the mesh of the total displacements that can be seen in Figure 5.28 the deformations differ from the Perniö embankment failure test. The deformations from the constant load indicated that there were mainly vertical displacements, which is an indication of high stability. In the Perniö embankment failure, horizontal displacements towards the ditch could be seen, however, in this scenario no or very small horizontal displacements occur by the ditch. The maximum displacement occurs directly under the embankment and reaches 0,52m. It can be seen that some deformations from consolidation occur on to the left and right of the embankment in addition to the deformations from the constant load.

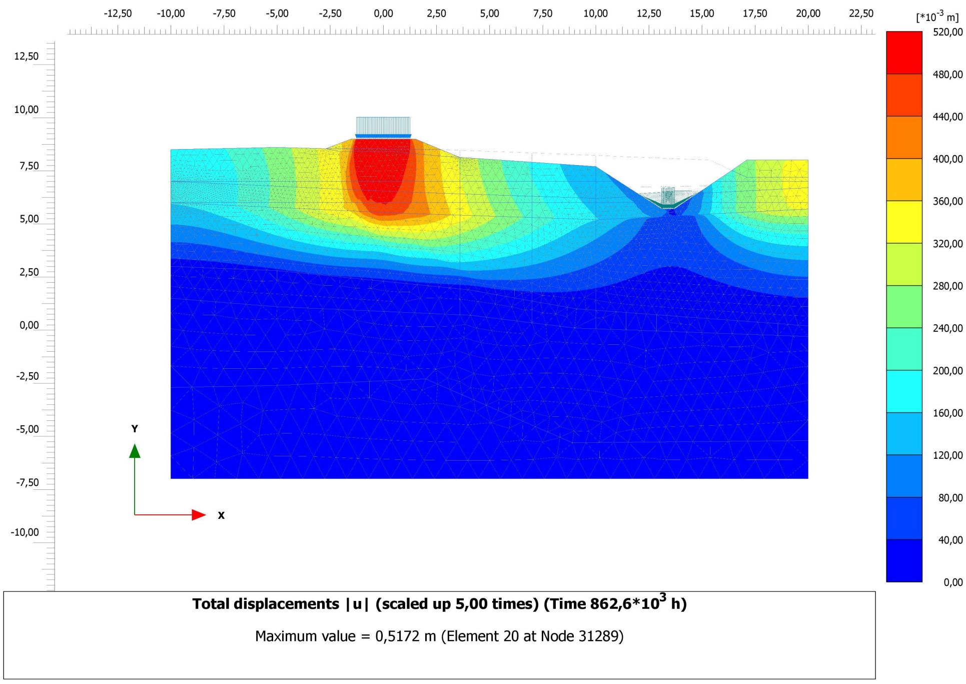

Figure 5.28: *Total displacement from train load 55kPa after 70 years*

The incremental displacements in figure 5.29 do not indicate any possible slip surfaces. However, it should be noted is that there seemed to be larger incremental displacements towards the right of the embankment in comparison to the failure test that had larger displacements towards the left of the embankment.

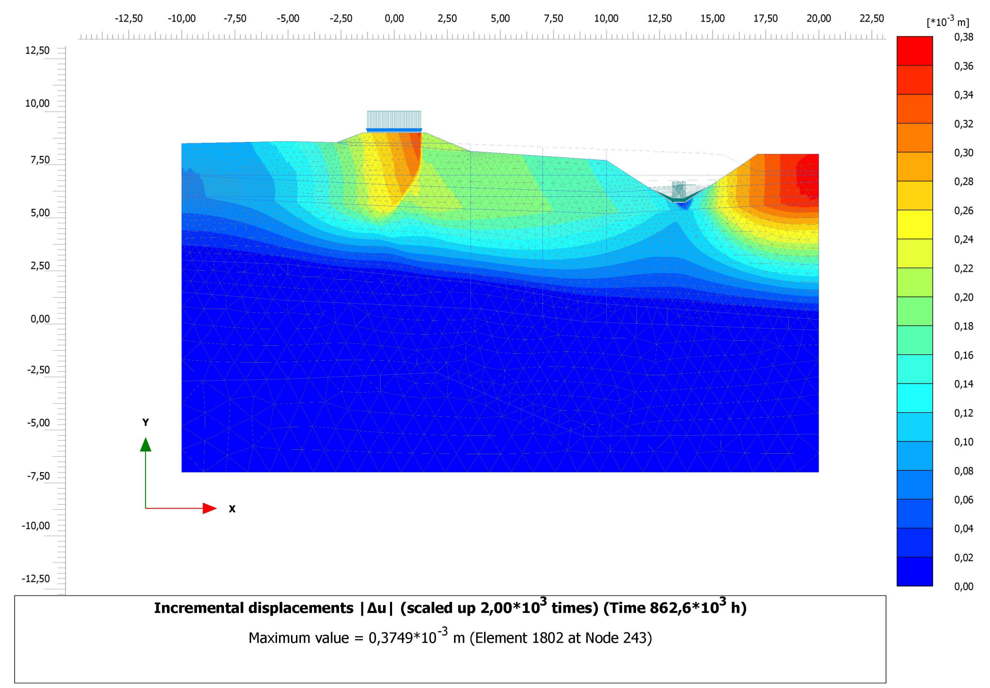

Figure 5.29: *Incremental displacement from train load 55kPa after 70 years*

The excess pore pressures were relatively small in the model since there was a long time of consolidation in the simulation. The largest excess pore pressures are in Clay layer 1 under the embankment and to the right of the ditch.

The simulation showed that the embankment will deform over time from a constant load of 55kPa. The deformations, however, were not of magnitude indicating that the embankment is near failure. The maximum displacement occurred by the embankment and reached 0.52m. This deformation may affect the performance of the railway in the case of a constant load of 55kPa. However, this scenario is seen as an extreme case and should not be considered as a possible scenario for a railway unless in constant use.

5.5.2 Train load, 71kPa

The scenario with a trainload of 71kPa was made to see if it was possible to have a lower safety factor than 1.3. The analysis was made in the same way as the scenario with a train standing still with a load of 55kPa, where the only difference is that the load in this scenario is increased to 71kPa.

The deformed mesh in Figure 5.30 shows the deformations after 70 years from a trainload of 71kPa. From the deformed mesh, it can be seen that deformations occur along the ground surface with larger deformations by the embankment. The maximum displacement reached 0.68m.

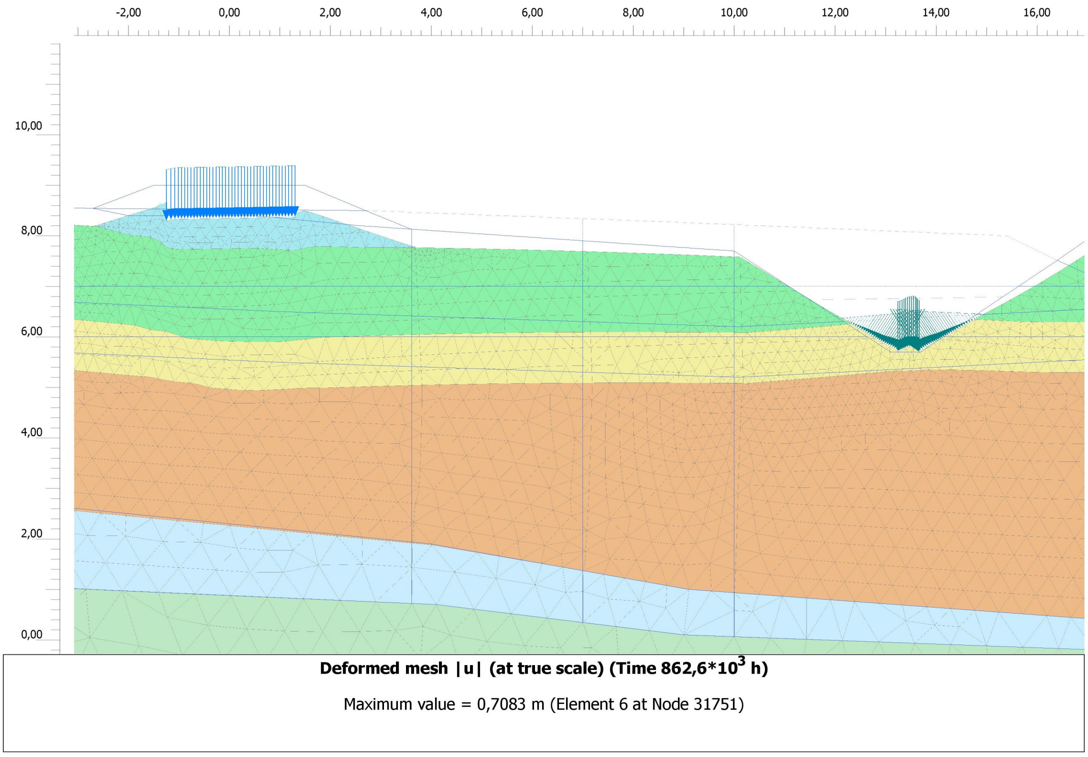

Figure 5.30: *Deformations from train load 71kPa after 70 years*

The total deformation mesh in Figure 5.31 indicates similar deformations to the Perniö embankment failure test. The deformations reached the ditch to the right of the embankment, however, these deformations are relatively small. The largest deformations are directly under the embankment. The maximum displacement is 0.72m. This is a relatively large deformation for an embankment.

The incremental displacements in Figure 5.32 do not indicate any slip surface for this scenario. This means that a failure similar to the Perniö embankment failure test is unlikely. The largest incremental displacements occur on the right side of the embankment, if the deformations to the right of the ditch are ignored.

The excess pore pressures were relatively small in the model. This since there has been a long time of consolidation in the simulation. The largest excess pore pressures are in Clay layer 1 under the embankment and to the right of the ditch.

The results from the simulation with a constant load of 71kPa showed similar results compared to the simulation with a constant load of 55kPa. The difference between the two simulations was the magnitude of deformations. The case with a constant load of 71kPa had a maximum displacement of 0.68m. This is 0.16m larger than the case with 55kPa. Also, the total displacement mesh presented in Figure 5.31 showed more similar displacements as the original simulated failure test with deformations towards the ditch. However, the simulation did not indicate a risk of failure.

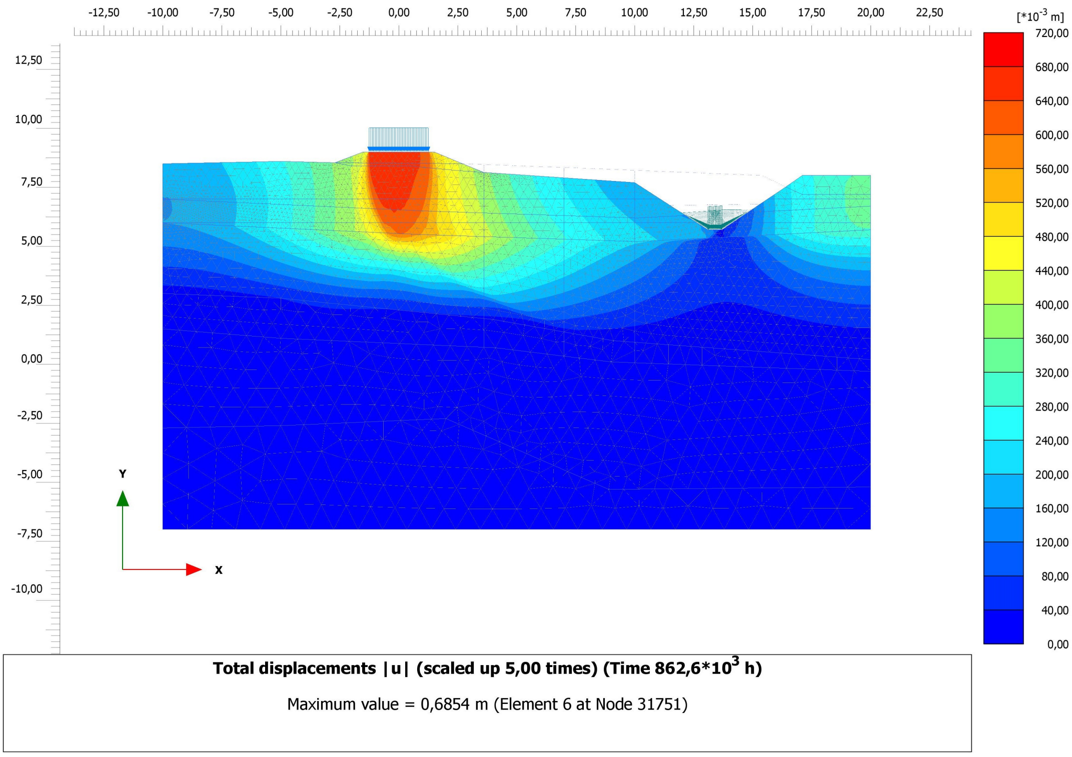

Figure 5.31: *Total displacement from train load 71kPa after 70 years*

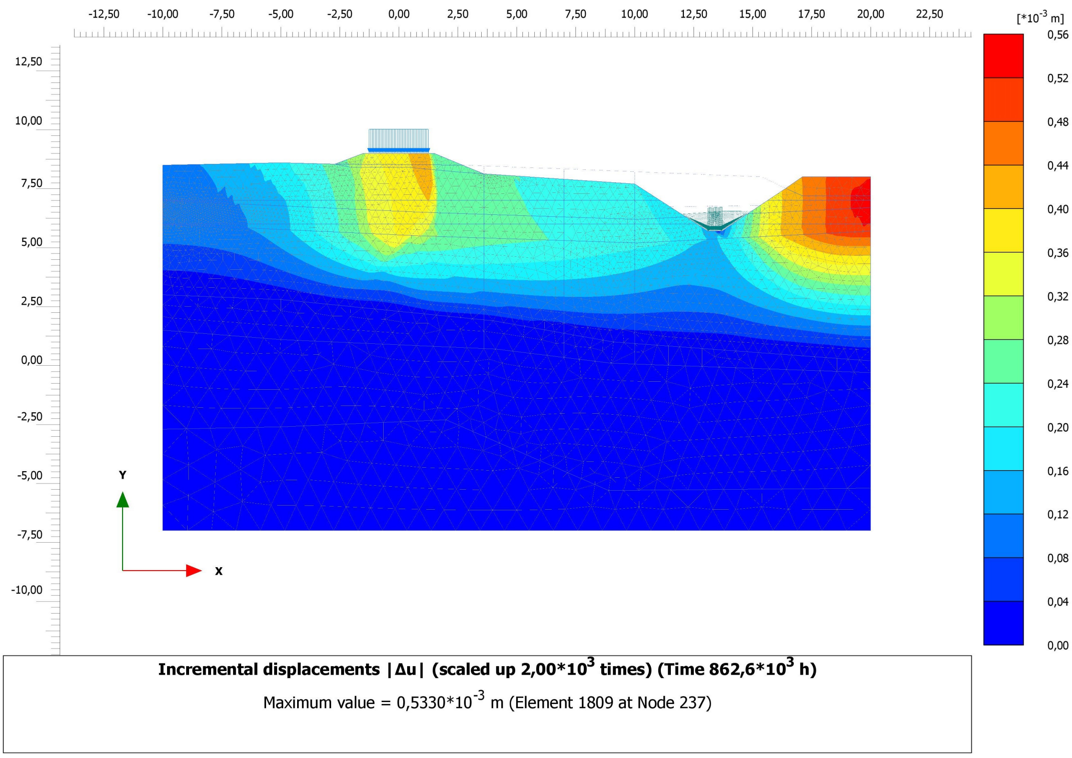

Figure 5.32: *Incremental displacement from trainload 71kPa after 70 years*

6
Conclusion

When modelling soil behaviour, numerical modelling is a useful tool. Even though in this thesis the simulated predictions were similar to the measured in situ results, numerical modelling is still an approximation. There are uncertainties when modelling soil behaviour, and choosing an appropriate model and inserting the correct input parameters is crucial in a numerical model.

When analysing failure cases, finite element method analyses may not be the best tools to use, this since FEM is based on equilibrium. In a real case, failure may thus occur before failure in the numerical model. This since Plaxis tolerates deformations to a higher degree than in a real case scenario, and there are always details (such as the stiffness of the instrumentation itself) that will be ignored in the numerical analyses. Also, the complexity and variability of the soil response should not be underestimated. Even though the Creep S-CLAY1S model is an advanced model, which takes most features of soft clay behaviour into consideration, despite there are still important parameters to take into consideration when analyzing simulated predictions.

When simulating a failure of an embankment with the Plaxis tool, the tool calculates until failure occurs in the soil controlled by the numerical input parameters. In a real case, the failure may occur earlier since the failure mechanism is not identical. The reason is that the soil starts moving due to consolidation and creep and causes disturbance on the ground. In the Perniö embankment test case, when the soil starts moving, the containers did collapse unlike in the model setup where a line load represented the containers.

The results also demonstrate that the predictions by a creep model are extremely sensitive to the assumed pre-consolidation pressure, and thus the initial state.
One important result the thesis ended with is that the model for the failure embankment is very sensitive for changes in parameters. This indicates the credibility of the model.

From the predictions based on the Plaxis simulation of the Perniö failure embankment, no need for reinforcement is necessary if a new railway is to be constructed on top of the Perniö embankment. The additional simulations with constant loads over a long time period predicted relatively large displacements, however, the simulated predictions showed no risk of failure in these scenarios.

An advantage of analysing failure with numerical models is cost saving. Setting up a numerical model in Plaxis is a much cheaper alternative than setting up a full-scale failure test, also, various scenarios can be easily studied. However, to get a reliable model with the correct input parameters, a detailed site investigation program is needed. Furthermore, the parameters need to be calibrated against the laboratory results before running the analyses, to retrieve reliable results.

Bibliography

Almeida, M. d. S. S., & Marques, M. E. S. (2013). *Design and Performance of Embankments on Very Soft Soils*. https://doi.org/10.1201/b15788

Amavasai, A., & Karstunen, M. (2017). BEST SOIL: Soft soil modelling and parameter determination MINNA KARSTUNEN AMARDEEP AMAVASAI.

D'Ignazio, M., Länsivaara, T. T., & Jostad, H. P. (2017). Failure in anisotropic sensitive clays: Finite element study of Perniö failure test. *Canadian Geotechnical Journal*, *54*(7), 1013–1033. https://doi.org/10.1139/cgj-2015-0313

Eckhardt, J., & Rantala, J. (2012). The Role of Intelligent Logistics Centres in a Multimodal and Cost-effective Transport System. *Procedia - Social and Behavioral Sciences*, *48*, 612–621. https://doi.org/10.1016/j.sbspro.2012.06.1039

Janbu, N. (1969). The resistance concept applied to deformations of soils. *Proc. 7th International Conference on soil mechanics.*

Karstunen, M., & Koskinen, M. (2008). Plastic anisotropy of soft reconstituted clays. *Canadian Geotechnical Journal*, *45*(3), 314–328. https://doi.org/10.1139/T07-073

Karstunen, M., Krenn, H., Wheeler, s. J., & Koskinen, M. (2005). Effect of anisotropy and destructuration on the behavior of Murro Test Embankment, *3641*(11), 2–3. https://doi.org/10.1061/(ASCE)1532-3641(2005)5

Karstunen, M., Wiltafsky, C., Krenn, H., Scharinger, F., & Schweiger, H. F. (2006). Modelling the behaviour of an embankment on soft clay with different constitutive models. *International Journal for Numerical and Analytical Methods in Geomechanics*, *30*(10), 953–982. https://doi.org/10.1002/nag.507

Larsson, R. (2008). Jords egenskaper. *Statens geotekniska institut (SGI)*, (5), 62.

Lehtonen, V. J., Meehan, C. L., Länsivaara, T. T., & Mansikkamäki, J. N. (2015). Full-scale embankment failure test under simulated train loading. *Geotechnique*, *65*(12), 961–974. https://doi.org/10.1680/jgeot.14.P.100

Leoni, M., Karstunen, M., & Vermeer, P. A. (2008a). Anisotropic creep model for soft soils. *Geotechnique*. https://doi.org/10.1680/geot.2008.58.3.215

Leoni, M., Karstunen, M., & Vermeer, P. A. (2008b). Anisotropic creep model for soft soils. *Geotechnique*. https://doi.org/10.1680/geot.2008.58.3.215

Lethonen, V. (2011). Instrumentation and analysis of railway embankment failure experiment - a general summary, 52 p.

Mansikkamäki, J. (2015). *Effective Stress Finite Element Stability Analysis of an Old Railway Embankment on Soft Clay* (Doctoral dissertation Vol. 1287).

Mataić, I. (2016). *On st ruc t ure and rat de pe nde nc e o f P e rniö c l ay.*

Mats Olsson. (2010). Calculating long-term settlement in soft clays –, 111.

Meijer, K., & Åberg, A. (2007). Krypsättningar i lera.

PLAXIS Material Models CONNECT Edition V20. (2015). In *Plaxis handbook*.

Sivasithamparam, N., Karstunen, M., & Bonnier, P. (2015). Modelling creep behaviour of anisotropic soft soils. *Computers and Geotechnics*, *69*, 46–57. https://doi.org/10.1016/j.compgeo.2015.04.015

svanø, G., C. S. N. N.S. (1991). A soil model for consolidation and creep. *PRoceeding of the 10th ecse, firenze*, 269–272.

Vozniak, E., Burgundosova, A., & Kopytova, A. (2018). Adaptation and reconstruction of the stations on the Finland railway road. *MATEC Web of Conferences*, *239*, 0–4. https://doi.org/10.1051/matecconf/201823901016

Wood, D. (1990). *Soil behaviour and critical State soil mechanics*.

Yin, Z. Y., Chang, C. S., Karstunen, M., & Hicher, P. Y. (2010). An anisotropic elastic-viscoplastic model for soft clays. *International Journal of Solids and Structures*, *47*(5), 665–677. https://doi.org/10.1016/j.ijsolstr.2009.11.004